On the Cross-Layer Restoration to Address Packet Layer Failures in P2MP-TRX-based WSONs

MEIHAN WU[1], XIAOLIANG CHEN[1*], FRANCESCO MUSUMECI[2], RUOXING LI[1], YUXIAO ZHANG[1], QIAN LV[1], AND ZUQING ZHU[1]

[1] *School of Information Science and Technology, University of Science and Technology of China, Hefei, P. R. China*
[2] *Politecnico di Milano, Milan, Italy*
[*] *xlichen@ieee.org*

Compiled October 29, 2024

Digital subcarrier multiplexing (DSCM) based coherent point-to-multipoint transceivers (P2MP-TRXs) are promising for addressing the shift in traffic patterns from point-to-point (P2P) to hub-and-spoke (H&S), and their application in wavelength-switched optical networks (WSONs) can potentially offer enhanced flexibility and efficiency in handling the mixed traffic therein. In this paper, we study how to secure the survivability of P2MP-TRX-based WSONs against packet layer failures with cross-layer restoration (CLR). By analyzing the unique features of P2MP-TRXs, we first design three CLR strategies to restore the traffic affected by packet layer failure(s) and then formulate an integer linear programming (ILP) model to leverage them for cost-effective CLR, *i.e.*, minimizing the cost introduced during the CLR process. Next, we propose a time-efficient heuristic, namely, hHAG-DP, which leverages hybrid dynamic programming (DP) and a hierarchical auxiliary graph (HAG) to find cost-effective CLR schemes quickly. Extensive simulations confirm the effectiveness of our proposals.

http://dx.doi.org/10.1364/ao.XX.XXXXXX

1. INTRODUCTION

With the popularization of 5G, emerging applications such as edge computing, Internet-of-things (IoT) and artificial intelligence (AI) are changing the pattern of Internet traffic [1–5] by replacing more and more point-to-point (P2P) traffic with hub-and-spoke (H&S) traffic, creating new challenges on network planning, bandwidth provisioning, and quality-of-service (QoS) guarantee [6, 7]. Therefore, communication service providers (CSPs) have been committed to seeking new optical network architectures to address these challenges [8–11], such that the increasing H&S traffic can be supported in a more flexible, efficient, reliable, and cost-effective manner.

This promotes the research and development (R&D) on coherent point-to-multipoint transceivers (P2MP-TRXs) [12], which leverage digital subcarrier multiplexing (DSCM) to distribute the data of high-speed H&S streams over the subcarrier (SC) channels targeted to different destinations. For example, the hub node in Fig. 1(a) fits 16 spectrally-adjacent SCs, each of which occupies bandwidth of 4 GHz, into a 75-GHz wavelength channel. Then, the SCs are allocated to leaf nodes according to the actual bandwidth demand between each hub-leaf pair, while each SC can be encoded, modulated/demodulated, and transmitted independently to form an efficient P2MP architecture for H&S traffic. As the unit cost of P2MP-TRXs is comparable to that of P2P-TRXs at the same data-rate [13], introducing P2MP-TRXs can significantly reduce capital expenditures (CAPEX) and operating expenses (OPEX), and simplify network control and management (NC&M) [14]. For instance, compared with the P2P-based solution in Fig. 1(c) that needs 5 TRXs on the hub node, the P2MP-TRX-based solution in Fig. 1(a) only needs one TRX on the hub node to support the same volume of H&S traffic.

The broadcast-and-select nature of P2MP-TRXs makes it easy for them being integrated with filterless optical networks (FONs) [15, 16], as shown in Fig. 1(b), especially for metro-aggregation networks [14]. Although FON simplifies network design and configuration by removing as many filtering and switching components as possible, it can hardly achieve relatively high spectrum utilization and lacks the flexibility to adjust spectrum allocation dynamically during operation. More importantly, it is vulnerable to physical-layer attacks (*e.g.*, high-power jamming and eavesdropping [17, 18]) due to the lack of ability to isolate and intercept malicious wavelengths at intermediate nodes. These intrinsic drawbacks can severely offset the benefits brought by P2MP-TRXs, motivating researchers to consider the implementation of P2MP-TRXs in wavelength-switched optical networks (WSONs) [19–21]. Note that, spectral resolutions at the FS-level have already been realized with fiber Bragg gratings decades ago [22–24], while the recent advances in commercial wavelength selective switches (WSS') based on liquid crystals on silicon further reduce the spectral granularity from 12.5 GHz to even 3.125

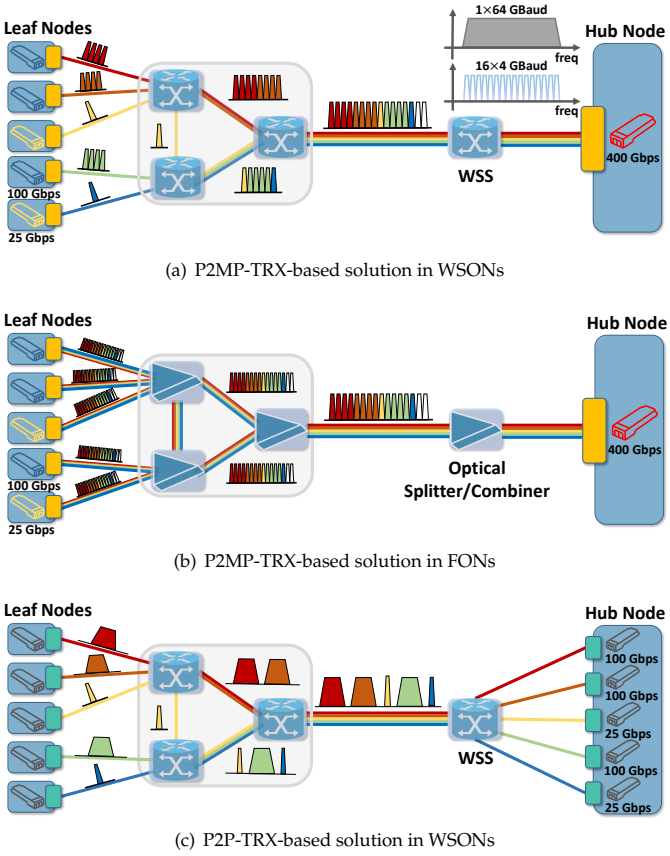

(a) P2MP-TRX-based solution in WSONs

(b) P2MP-TRX-based solution in FONs

(c) P2P-TRX-based solution in WSONs

Fig. 1. Provisioning H&S traffic with P2MP-TRXs and P2P-TRXs.

GHz [25]. Hence, these optical switching technologies facilitate P2MP-TRX-based WSONs, providing new opportunities to explore the benefits of P2MP-TRXs in spectral-efficient and adaptive optical networks with mixed metro/core traffic [21].

As the studies on P2MP-TRX-based WSONs are still in the early stage, a few key issues have not been fully explored yet, particularly, network survivability. A WSON can be impacted by failures in both the optical layer (*e.g.*, optical impairments and fiber cuts [26, 27]) and the packet layer (*e.g.*, switch/router outages [28]). Existing studies have already considered how to address optical layer failures [16, 19], but to the best of our knowledge, how to restore a P2MP-TRX-based WSON from packet layer failures has not been tackled in the literature, except for our own preliminary work in [29]. Indeed, packet layer failures actually happen much more frequently than optical layer ones in large production WSONs, and ∼80% of them cannot be repaired immediately and can last for 10-100 minutes, according to Google's analysis [30]. Therefore, overlooking packet layer failures will result in unpredictable data and revenue losses to CSPs.

Note that, packet layer failures normally cannot be restored with the protection and restoration strategies designed for the optical layer. This can be illustrated by the example in Fig. 2. Here, we have a flow that should be forwarded from *Switch* 1 to *Switch* 3, and its routing path is 1→2→3 in the packet layer. In the optical layer, the working lightpaths for 1→2 and 2→3 are marked with green solid lines, which are protected by dedicated path protection (*i.e.*, the backup lightpaths labeled by red dashed

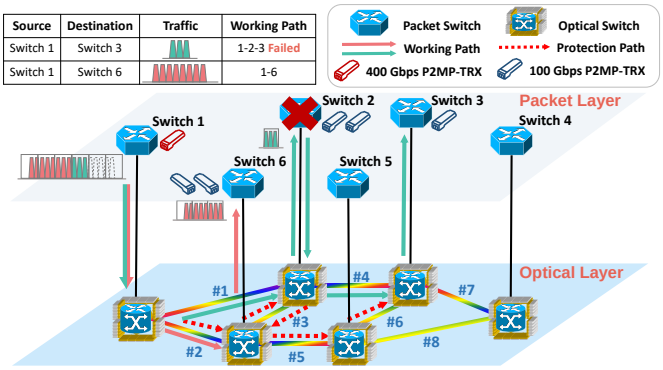

Fig. 2. Example on packet layer failure in a P2MP-TRX-based WSON.

lines). However, if *Switch* 2 is broken, the service of the flow will be interrupted regardless of the protection in the optical layer. This is because such a packet layer failure is beyond the scope of protection or recovery measures designed solely for the optical layer. Meanwhile, the conventional routing backup strategies and fast rerouting policies tailored for packet layer failures [31] fail to consider the unique features of P2MP-TRXs and thus cannot efficiently utilize resources in a P2MP-TRX-based WSON. Therefore, cross-layer restoration (CLR) [32, 33] should be leveraged to solve the problem more cost-effectively. Nevertheless, efficient CLR algorithms cannot be designed without incorporating the unique features of P2MP-TRXs [29].

In this work, we significantly expand our preliminary study in [29] to better answer how to design CLR to recover a P2MP-TRX-based WSON from packet layer failure(s) cost-effectively. We first analyze the unique features of P2MP-TRXs to optimize the three CLR strategies designed in [29]: 1) rerouting with in-service P2MP-TRXs, 2) rerouting with reconfigured P2MP-TRXs and lightpaths, and 3) activating idle P2MP-TRXs and establishing new lightpaths. Then, we extract all the traffic through the failed switch(es), and use it together with the network status after packet layer failure(s) and the three CLR strategies as inputs to formulate an integer linear programming (ILP) model for recovering all the affected traffic with minimized CLR cost, which includes the costs of new hub/leaf P2MP-TRXs, new frequency slots (FS'), and reconfiguring in-service P2MP-TRXs. Next, to solve the problem time-efficiently, we propose a novel heuristic based on hybrid dynamic programming (DP) and a hierarchical auxiliary graph (HAG), namely, hHAG-DP. Finally, we evaluate our proposals with extensive simulations and verify that hHAG-DP outperforms the algorithms designed in [29].

The rest of the paper is organized as follows. Section 2 briefly surveys the related work. We explain the network model and three CLR strategies in Section 3. The ILP model and the hHAG-DP algorithm are described in Sections 4 and 5, respectively. In Section 6, we discuss the performance evaluations. Finally, Section 7 summarizes the paper.

2. RELATED WORK

DSCM-based P2MP-TRXs are promising devices to improve the flexibility, cost-effectiveness, scalability, and reconfigurability of next-generation optical networks. Welch *et al.* [12] provided the first comprehensive explanation of the operation principle and pivotal elements of P2MP-TRXs and discussed in depth about the cost reduction that they could achieve over

P2P-TRXs. Later on, in [13], they experimentally demonstrated to realize a software-reconfigurable optical network with P2MP-TRXs. Then, to explore the benefits of P2MP-TRXs, people have considered how to plan P2MP-TRX-based FONs in [14, 34–36]. Specifically, the studies in [34–36] tackled the network planning of P2MP-TRX-based FONs in ring and horseshoe topologies, while the authors of [14] approached the deployment of P2MP-TRX-based FONs from a long-term planning perspective and proposed a multi-period planning scheme to reduce costs. Researchers have also tried to improve the survivability of P2MP-TRX-based FONs [16, 37]. In [37], the cost savings brought by P2MP-TRXs were compared in protection and non-protection scenarios. Lv *et al.* [16] designed algorithms for survivable multilayer planning of P2MP-TRX-based FONs. In addition to network planning, dynamic service provisioning was also considered for P2MP-TRX-based FONs [38–40].

As for P2MP-TRX-based WSONs, the existing studies in the literature are much fewer than those on P2MP-TRX-based FONs. Pavon-Marino *et al.* [20] formulated the network planning of P2MP-TRX-based WSONs as a tree-determination, routing, and spectrum assignment problem and solved it effectively. The study in [21] proposed network planning algorithms that jointly optimize SC allocation and routing and spectrum assignment (RSA) to minimize the CAPEX of P2MP-TRX-based WSONs. The authors of [41] addressed dynamic service provisioning in P2MP-TRX-based WSONs and proposed a scheme to optimize resource utilization by leveraging SC-level reconfiguration. In [19], we studied the survivable network planning of P2MP-TRX-based WSONs to address single-link failures, and explained the differences from its counterparts in elastic optical networks (EONs) [42–45] and why it should be revisited. Finally, our preliminary work in [29] designed three CLR strategies to recover P2MP-TRX-based WSONs from packet layer failures, but we have not formulated an ILP model to solve the problem exactly and the proposed heuristics can be further improved as we will explain later in this paper.

3. OPERATION PRINCIPLE

In this section, we first introduce the network model of P2MP-TRX-based WSONs, and then elaborate on the three CLR strategies designed to address packet layer failures.

A. Network Model

Fig. 2 shows an example on P2MP-TRX-based WSONs, which consists of both packet and optical layers. We model such a P2MP-TRX-based WSON as a graph $G(V, E)$, where V and E respectively represent the nodes and fiber links. In the packet layer, each node $v \in V$ contains a packet switch, on which hub and leaf P2MP-TRXs can be activated as needed. We denote the type sets of hub and leaf P2MP-TRXs as T_{H} and T_{L} (in terms of capacities), respectively, and as certain P2MP-TRXs can be used as either hubs or leaves [12], T_{H} and T_{L} are partially intersect ($T_{\mathrm{H}} \cap T_{\mathrm{L}} \neq \emptyset$). However, we do not consider switching the role of a P2MP-TRX once it has been activated. We follow the setting in [12] to assume that the bandwidth of each SC is 4 GHz and the modulation format of each SC can be adaptively selected between DP-QPSK and DP-16QAM according to the transmission distance. Specifically, an SC can use DP-16QAM to achieve a capacity of 25 Gbps if the transmission distance does not exceed 500 km, and it will deliver 12.5 Gbps with DP-QPSK, otherwise. In the optical layer, each node contains an optical switch, which connects to its local packet switch and can realize FS-level switching (each FS occupies 12.5 GHz) with SC-level guard-bands (vacant SCs reserved at edges of FS′ to be switched by WSS′ [21]) to set up lightpaths, *i.e.*, the optical layer is essentially a flexible-grid EON [8]. Due to the misalignment between the FS and SC bandwidth, SCs might not always neatly fall in different FS′ as showcased by Fig. 3.

In the P2MP-TRX-based WSON, all the traffic is between switches in the packet layer. We model the traffic between two switches s_i and d_i as $r_i(s_i, d_i, x_i)$, where i is its unique index and x_i denotes its bandwidth (in SCs assuming that DP-16QAM is used), and for simplicity, we can refer the traffic r_i as a flow. The transmission of each flow r_i in the P2MP-TRX-based WSON needs to satisfy constraints in both the packet and optical layers. As for the packet layer, we need to allocate SCs on pair(s) of hub/leaf P2MP-TRXs to provision the bandwidth x_i of r_i, while the SCs allocated on each pair of hub/leaf P2MP-TRXs should satisfy the SC non-overlapping, contiguity, and continuity constraints [21]. In this work, we do not apply multipath routing (*i.e.*, bifurcating a flow over multiple paths) because it would impose differential delay constraints that can significantly complicate the algorithm and system designs. As for the optical layer, we need to allocate FS′ on fiber links to establish the lightpath between each pair of hub/leaf P2MP-TRXs, satisfying the spectrum non-overlapping, contiguity, and continuity constraints [8]. Each failed switch in the packet layer can interrupt the flows that it was forwarding as an intermediate switch, and we point out that if a flow uses the failed switch as its source or destination, the flow cannot be restored before the switch has been repaired [32]. Therefore, the affected flows that are restorable can be obtained by checking each failed switch, and they will be put into set $\mathbf{R}$, which will be recovered with CLR.

B. CLR Strategies

To restore all the affected flows in $\mathbf{R}$ cost-effectively, we design three CLR strategies to fully utilize the idle resources in a P2MP-TRX-based WSON after packet layer failure(s) to reroute them through joint consideration of SCs on P2MP-TRXs and FS′ on fiber links.

The first CLR strategy checks all the feasible lightpaths based on the current network condition and leverages the idle SCs on in-service P2MP-TRXs to reroute an affected flow in $\mathbf{R}$. Fig. 3(a) provides an example on this strategy. Here, the bandwidth of $r_i \in \mathbf{R}$ is $x_i = 75$ Gbps. We first determine the restoration path as 1→3 in the packet layer, using a new lightpath over 1→6→5→3 in the optical layer, which contains enough available FS′. We assume that the length of the lightpath is within 500 km, and thus r_i can be carried with 3 SCs using DP-16QAM. Then, as the in-service P2MP-TRXs at s_i and d_i (*Switches* 1 and 3) still have enough idle SCs for r_i and the corresponding FS′ on fiber links of the new lightpath are also unused, we can just restore r_i with the P2MP-TRXs. Note that, in the case when the bandwidth of r_i is less than the capacity of an SC, we still restore it with a new SC rather than seeking free capacities from activated SCs.

If the bandwidth of r_i is 150 Gbps and all the other settings stay unchanged, it cannot be recovered with the first CLR strategy and we have to reconfigure the two in-service P2MP-TRXs on *Switches* 1 and 3 to use a new central frequency. Fig. 3(b) explains the details about the second CLR strategy. Specifically, as rerouting r_i will need 6 SCs and thus 2 FS′ on fiber links, the available FS′ on *Links* 5 and 6 become insufficient if the P2MP-TRXs still use their original central frequency. Hence, we first reconfigure the P2MP-TRXs to use the new central frequency that corresponds to sufficient FS′ over 1→6→5→3, and then

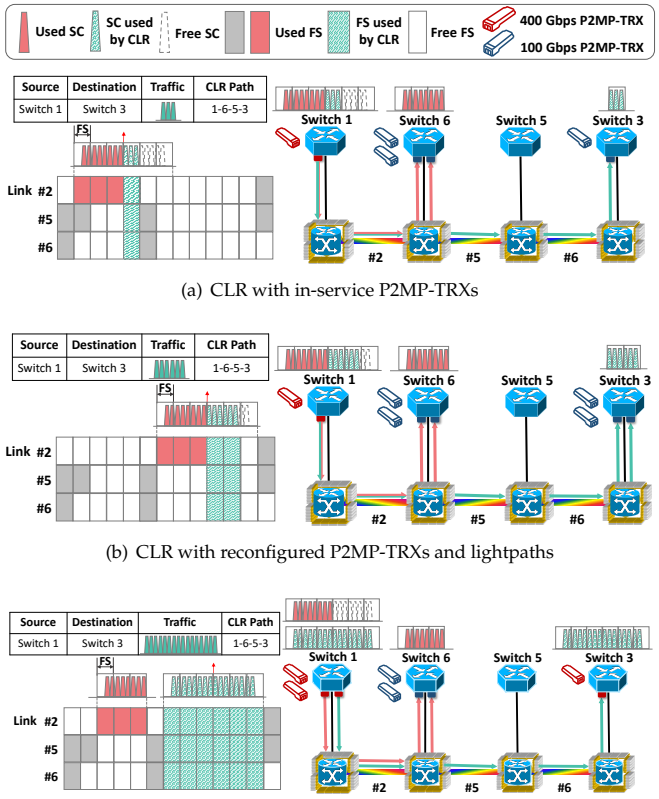

(a) CLR with in-service P2MP-TRXs

(b) CLR with reconfigured P2MP-TRXs and lightpaths

(c) CLR by activating new P2MP-TRXs and lightpaths

Fig. 3. Three CLR strategies for restoring affected traffic.

restore r_i accordingly. Note that, in this case, the in-service lightpath between *Switches* 1 and 6 (marked in red in Fig. 3(b)) is also reconfigured.

The third CLR strategy will be used if the first two strategies are infeasible. As shown in Fig. 3(c), if the bandwidth of r_i increases to 400 Gbps, we cannot accommodate it with in-service P2MP-TRXs anymore. Therefore, we will activate two unused P2MP-TRXs on *Switches* 1 and 3 to establish direct end-to-end lightpaths for restoring r_i.

The costs of the three CLR strategies mainly comes from the costs of newly-activated P2MP-TRXs, newly-used FS', and reconfiguring in-service P2MP-TRXs. Hence, we define the unit costs of a type-t ($t \in T_{\mathrm{H}} \cup T_{\mathrm{L}}$) P2MP-TRX, an FS, and a P2MP-TRX reconfiguration as Δ_t, Δ_f and Δ_r, respectively. Then, the costs of the CLR strategies can be quantified as

$$\mathbf{C} = \begin{cases} \sum\limits_{t \in T_{\mathrm{L}}} n_t^{\mathrm{L}} \cdot \Delta_t + n_{\mathrm{FS}} \cdot \Delta_f, & \text{First,} \\ \sum\limits_{t \in T_{\mathrm{L}}} n_t^{\mathrm{L}} \cdot \Delta_t + n_{\mathrm{FS}} \cdot \Delta_f + n_{\mathrm{R}} \cdot \Delta_r, & \text{Second,} \\ \sum\limits_{t \in T_{\mathrm{L}} \cup T_{\mathrm{H}}} (n_t^{\mathrm{L}} + n_t^{\mathrm{H}}) \cdot \Delta_t + n_{\mathrm{FS}} \cdot \Delta_f, & \text{Third,} \end{cases} \quad (1)$$

where n_t^{L} and n_t^{H} denote the numbers of newly-activated leaf and hub P2MP-TRXs in type-t, respectively, n_{FS} is the number of newly-used FS', and n_{R} is the number of P2MP-TRX reconfigurations (*i.e.*, frequency shifts). In Eq. (1), we do not count the cost of newly-activated hub P2MP-TRXs for the first and second CLR strategies, because as shown in Figs. 3(a) and 3(b), they just reuse the original in-service hub P2MP-TRX before packet layer failure(s) to restore each flow. Meanwhile, there might be additional leaf P2MP-TRXs when using these two CLR strategies, since rerouting can use a longer lightpath, which might change the modulation format and thus increase the required SCs to a value that cannot be accommodated by the original leaf P2MP-TRX (*i.e.*, an idle leaf P2MP-TRX needs to be activated at the destination).

4. ILP MODEL

In this section, we formulate an ILP model to leverage the three CLR strategies discussed above to restore a P2MP-TRX-based WSON from packet layer failure(s) cost-effectively.

Notations:

- $G(V, E)$: the network topology, where V and E are the sets of nodes and fiber links, respectively.
- $\mathbf{R}$: the set of affected flows after packet layer failure(s), where each flow $r_i \in \mathbf{R}$ is denoted as $r_i(s_i, d_i, x_i)$.
- $\tilde{\mathbf{R}}$: the set of unaffected flows after packet layer failure(s).
- $g_{u,v}$: the indicator that equals 1 if there is at least one lightpath between nodes u and v, and 0 otherwise.
- $d_{u,v}$: the length of fiber link $e = (u, v) \in E$.
- $U_v^{\mathrm{H}}/U_v^{\mathrm{L}}$: the sets of hub/leaf P2MP-TRXs on node $v \in V$.
- $\tilde{U}_v^{\mathrm{H}}/\tilde{U}_v^{\mathrm{L}}$: the sets of in-service hub/leaf P2MP-TRXs on node $v \in V$ before CLR.
- $T_{\mathrm{H}}/T_{\mathrm{L}}$: the type sets of hub/leaf P2MP-TRXs.
- N_p: the set of SCs on a P2MP-TRX p.
- $\tilde{q}_{u,v}^i$: the indicator that equals 1 if unaffected flow $r_i \in \tilde{\mathbf{R}}$ uses a lightpath between nodes u and v, and 0 otherwise.
- $\tilde{\theta}_{v,p,i}^{\mathrm{H}}/\tilde{\theta}_{v,p,i}^{\mathrm{L}}$: the indicators that equal 1 if flow $r_i \in \tilde{\mathbf{R}}$ uses a hub/leaf P2MP-TRX p on node v, and 0 otherwise.
- $\tilde{\xi}_{p,t,v}^{\mathrm{H}}/\tilde{\xi}_{p,t,v}^{\mathrm{L}}$: the indicators that equal 1 if a hub/leaf P2MP-TRX p on node v is of type-t and is used before CLR, and 0 otherwise.
- C_t: the capacity of a type-t P2MP-TRX in SCs.
- $\tilde{z}_{v,p,i}^{\mathrm{S}}/\tilde{z}_{v,p,i}^{\mathrm{E}}$: the start/end indices of SCs used by unaffected flow $r_i \in \tilde{\mathbf{R}}$ on hub P2MP-TRX p on node v.
- $\tilde{f}_{v,p}^{\mathrm{H,S}}$: the start index of FS' used by a hub P2MP-TRX p on node v before CLR.
- $\tilde{f}_i^{\mathrm{S}}/\tilde{f}_i^{\mathrm{E}}$: the start/end indices of FS' used by flow $r_i \in \tilde{\mathbf{R}}$.
- $\tilde{p}_i^{\mathrm{H}}$: the hub P2MP-TRX used by unaffected flow $r_i \in \tilde{\mathbf{R}}$.
- $\Delta f_{t,s}^{\mathrm{S}}/\Delta f_{t,s}^{\mathrm{E}}$: the FS shifts (from the start FS) of the start/end SC s of an SC block on a type-t P2MP-TRX.
- M: a very large constant.
- F: the maximum index of FS' on a fiber link.
- $\mathcal{F}$: the number of used FS' before CLR.
- $\Delta_t/\Delta_f/\Delta_r$: the unit costs of hub/leaf P2MP-TRXs of type-t/FS'/P2MP-TRX reconfiguration, respectively.

Variables:

- $q^{i}_{u,v}$: the boolean variable that equals 1 if flow $r_i \in \mathbf{R} \cup \tilde{\mathbf{R}}$ uses fiber link $e = (u, v) \in E$ after CLR, and 0 otherwise.
- l_i: the path length of affected flow $r_i \in \mathbf{R}$ after CLR.
- m_i: the boolean variable that equals 1 if affected flow r_i is recovered with a lightpath using DP-16QAM, and 0 if its lightpath uses DP-QPSK.
- sc_i: the number of SCs for affected flow r_i after CLR.
- $\theta^{\mathrm{H}}_{v,p,i}/\theta^{\mathrm{L}}_{v,p,i}$: the boolean variable that equals 1 if flow $r_i \in \mathbf{R} \cup \tilde{\mathbf{R}}$ uses a hub/leaf P2MP-TRX p on node v after CLR, and 0 otherwise.
- $\rho^{\mathrm{H}}_{v,p}/\rho^{\mathrm{L}}_{v,p}$: the boolean variable that equals 1 if hub/leaf P2MP-TRX p on node v is used, and 0 otherwise.
- $\xi^{\mathrm{H}}_{p,t,v}/\xi^{\mathrm{L}}_{p,t,v}$: the boolean variable that equals 1 if hub/leaf P2MP-TRX p on node v is of type-t and it is used after CLR, and 0 otherwise.
- $C^{\mathrm{H}}_{v,p}/C^{\mathrm{L}}_{v,p}$: the capacities of hub/leaf P2MP-TRX p on node v (in SCs) after CLR.
- $\alpha^{p}_{i,j}$: the boolean variable that equals 1 if affected flow r_i shares hub P2MP-TRX p with flow r_j, and 0 otherwise.
- $z^{\mathrm{S}}_{v,p,i}/z^{\mathrm{E}}_{v,p,i}$: the start/end indices of SCs used by flow $r_i \in \mathbf{R} \cup \tilde{\mathbf{R}}$ on hub P2MP-TRX p on node v.
- $sc_{i,v,p}$: the number of SCs used on leaf P2MP-TRX p on node v for affected flow r_i.
- $o^{p}_{i,j}$: the boolean variable that equals 1 if SCs used by affected flow r_i on hub P2MP-TRX p on its source s_i are after those used by flow r_j, and 0 otherwise.
- $f^{\mathrm{H,S}}_{v,p}$: the start index of FS' used by a hub P2MP-TRX p on node v after CLR, $f^{H,S}_{v,p} \geq 0$.
- $\pi_{v,p}$: the boolean variable that equals 1 if hub P2MP-TRX p on node v is reconfigured after CLR, and 0 otherwise.
- $z^{\mathrm{S}}_{p,t,v,i}/z^{\mathrm{E}}_{p,t,v,i}$: the start/end indices of SCs used by affected flow r_i on type-t hub P2MP-TRX p on node v.
- $\beta^{i,\mathrm{S}}_{t,p,v,s}/\beta^{i,\mathrm{E}}_{t,p,v,s}$: the boolean variable that equals 1 if the start/end index of SCs used by affected flow r_i on type-t hub P2MP-TRX p on node v is s, and 0 otherwise.
- $f^{\mathrm{H,S}}_{v,p,i}$: the start index of FS' used by hub P2MP-TRX p on node v for affected flow r_i.
- $f^{\mathrm{S}}_{v,p,i}/f^{\mathrm{E}}_{v,p,i}$: the start/end indices of FS' used by flow $r_i \in \mathbf{R} \cup \tilde{\mathbf{R}}$ on hub P2MP-TRX p on node v (within $[1, F]$).
- $f^{\mathrm{S}}_{u,v,i}/f^{\mathrm{E}}_{u,v,i}$: the start/end indices of FS' used by flow $r_i \in \mathbf{R} \cup \tilde{\mathbf{R}}$ on fiber link $e = (u, v) \in E$.
- $p^{\mathrm{H}}_{u,v,i}$: the unique index of the hub P2MP-TRX used by flow $r_i \in \mathbf{R} \cup \tilde{\mathbf{R}}$ for lightpath $u \rightarrow v$.
- $\eta^{i,j}_{u,v}$: the boolean variable that equals 0 if flows r_i and r_j share fiber link $e = (u, v) \in E$ and the same hub P2MP-TRX, and 1 otherwise.
- $w^{i,j}_{u,v}$: the boolean variable that equals 1 if FS' used by flow r_i on fiber link $e = (u, v) \in E$ are after those used by flow r_j, and 0 otherwise.
- $n^{\mathrm{H}}_{t}/n^{\mathrm{L}}_{t}/n_{\mathrm{FS}}/n_{\mathrm{R}}$: the total numbers of newly-activated hub/leaf P2MP-TRXs of type-t, newly-used FS', and P2MP-TRX reconfigurations, respectively.
- $\gamma^{i,j}_{u,v}$: the auxiliary integer variable for linearization.
- $\delta^{i,j}_{u,v}$: the auxiliary boolean variable for linearization.

Objective:

The objective is to minimize the total cost of CLR as

$$\text{Minimize} \quad \sum_{t \in T_{\mathrm{L}} \cup T_{\mathrm{H}}} (n^{\mathrm{L}}_{t} + n^{\mathrm{H}}_{t}) \cdot \Delta_t + n_{\mathrm{FS}} \cdot \Delta_f + n_{\mathrm{R}} \cdot \Delta_r, \tag{2}$$

where the first term represents the cost of newly-activated transceivers in various types, including both hub and leaf P2MP-TRXs, the second term denotes the cost of newly-used FS', and the last one conveys the cost of reconfiguring in-service P2MP-TRXs.

Constraints:

1) Constraints on Routing and Modulation Formats:

$$\sum_{v \in V} q^{i}_{u,v} - \sum_{v \in V} q^{i}_{v,u} = \begin{cases} 1, & s_i = u, \\ -1, & d_i = u, \\ 0, & \text{others}, \end{cases} \quad \{i : r_i \in \mathbf{R}\}, \tag{3}$$

$$\sum_{v \in V} q^{i}_{u,v} \leq 1, \quad \{i : r_i \in \mathbf{R}\}, \ \forall u \in V, \tag{4}$$

$$q^{i}_{u,v} \leq g_{u,v}, \quad \{i : r_i \in \mathbf{R}\}, \ \forall u, v \in V. \tag{5}$$

Eq. (3)-Eq. (5) ensure that each affected flow r_i is recovered with a single restoration path.

$$l_i = \sum_{u,v \in V} q^{i}_{u,v} \cdot d_{u,v}, \quad \{i : r_i \in \mathbf{R}\}, \tag{6}$$

$$\frac{l_i}{500} - m_i \leq (1 - m_i) \cdot M \leq \frac{l_i}{500} \cdot M - 1, \quad \{i : r_i \in \mathbf{R}\}. \tag{7}$$

Eq. (6) calculates the length of the restoration path of each affected flow r_i, and Eq. (7) ensures that the modulation format of the restoration lightpath is determined correctly.

$$sc_i = (2 - m_i) \cdot x_i, \quad \{i : r_i \in \mathbf{R}\}. \tag{8}$$

Eq. (8) calculates the number of SCs needed to restore each affected flow.

2) Constraints on Selecting P2MP-TRXs:

$$\theta^{\mathrm{H}}_{v,p,i} = \tilde{\theta}^{\mathrm{H}}_{v,p,i}, \quad \{i : r_i \in \tilde{\mathbf{R}}\}, \ \forall v \in V, \ p \in U^{\mathrm{H}}_{v}, \tag{9}$$

$$\theta^{\mathrm{L}}_{v,p,i} = \tilde{\theta}^{\mathrm{L}}_{v,p,i}, \quad \{i : r_i \in \tilde{\mathbf{R}}\}, \ \forall v \in V, \ p \in U^{\mathrm{L}}_{v}, \tag{10}$$

$$\begin{cases} \sum_{p \in U^{\mathrm{H}}_{v}} \theta^{\mathrm{H}}_{v,p,i} = 1, \ \sum_{p \in U^{\mathrm{L}}_{v}} \theta^{\mathrm{L}}_{v,p,i} = 0, & s_i = v, \\ \sum_{p \in U^{\mathrm{H}}_{v}} \theta^{\mathrm{H}}_{v,p,i} = 0, \ \sum_{p \in U^{\mathrm{L}}_{v}} \theta^{\mathrm{L}}_{v,p,i} \leq M, & d_i = v, \\ \sum_{p \in U^{\mathrm{H}}_{v}} \theta^{\mathrm{H}}_{v,p,i} = 0, \ \sum_{p \in U^{\mathrm{L}}_{v}} \theta^{\mathrm{L}}_{v,p,i} = 0, & \text{others}, \end{cases} \quad \{i : r_i \in \mathbf{R}\}. \tag{11}$$

Eq. (9)-Eq. (10) record the hub and leaf P2MP-TRXs used by each unaffected flow $r_i \in \tilde{\mathbf{R}}$, and Eq. (11) determines the hub and leaf P2MP-TRXs used to restore each affected flow $r_i \in \mathbf{R}$ on its source s_i and destination d_i, respectively. As the CLR only needs to restore the traffic affected by a failed packet switch, the

volume of the affected traffic would not be very large related to the overall network capacity. Hence, we do not consider the situation in which the number of available P2MP-TRXs is insufficient for CLR, *i.e.*, not limiting the maximum number of each type of P2MP-TRX that can be used.

$$\rho^{\mathrm{H}}_{v,p} \le \sum_{\{i:r_i\in\mathbf{R}\cup\tilde{\mathbf{R}}\}} \theta^{\mathrm{H}}_{v,p,i} \le \rho^{\mathrm{H}}_{v,p}\cdot M, \quad \forall v\in V,\ p\in U^{\mathrm{H}}_v, \tag{12}$$

$$\rho^{\mathrm{L}}_{v,p} = \sum_{\{i:r_i\in\mathbf{R}\cup\tilde{\mathbf{R}}\}} \theta^{\mathrm{L}}_{v,p,i}, \quad \forall v\in V,\ p\in U^{\mathrm{L}}_v. \tag{13}$$

Eq. (12)-Eq. (13) update the usage of hub and leaf P2MP-TRXs.

3) Constraints on Determining P2MP-TRX Types:

$$\xi^{\mathrm{H}}_{p,t,v} = \tilde{\xi}^{\mathrm{H}}_{p,t,v}, \quad \forall v\in V,\ p\in\tilde{U}^{\mathrm{H}}_v,\ t\in T_{\mathrm{H}}, \tag{14}$$

$$\xi^{\mathrm{L}}_{p,t,v} = \tilde{\xi}^{\mathrm{L}}_{p,t,v}, \quad \forall v\in V,\ p\in\tilde{U}^{\mathrm{L}}_v,\ t\in T_{\mathrm{L}}, \tag{15}$$

$$\sum_{t\in T_h} \xi^{\mathrm{H}}_{p,t,v} = \rho^{\mathrm{H}}_{v,p}, \quad \forall v\in V,\ p\in U^{\mathrm{H}}_v\setminus\tilde{U}^{\mathrm{H}}_v, \tag{16}$$

$$\sum_{t\in T_l} \xi^{\mathrm{L}}_{p,t,v} = \rho^{\mathrm{L}}_{v,p}, \quad \forall v\in V,\ p\in U^{\mathrm{L}}_v\setminus\tilde{U}^{\mathrm{L}}_v. \tag{17}$$

Eq. (14)-Eq. (17) determine the type of each hub/leaf P2MP-TRX used after CLR.

$$C^{\mathrm{H}}_{v,p} = \sum_{t\in T_h} \xi^{\mathrm{H}}_{p,t,v}\cdot C_t, \quad \forall v\in V,\ p\in U^{\mathrm{H}}_v, \tag{18}$$

$$C^{\mathrm{L}}_{v,p} = \sum_{t\in T_l} \xi^{\mathrm{L}}_{p,t,v}\cdot C_t, \quad \forall v\in V,\ p\in U^{\mathrm{L}}_v. \tag{19}$$

Eq. (18)-Eq. (19) determines the capacity of each hub/leaf P2MP-TRX used after CLR.

$$\begin{aligned} &\alpha^p_{i,j} \le \frac{1}{2}\cdot\left(\theta^{\mathrm{H}}_{v,p,i}+\theta^{\mathrm{H}}_{v,p,j}\right),\\ &\{i,j: r_i\in\mathbf{R}, r_j\in\mathbf{R}\cup\tilde{\mathbf{R}}, i\ne j, v=s_i\},\ \forall p\in U^{\mathrm{H}}_v. \end{aligned} \tag{20}$$

Eq. (20) identifies the flows that share the hub P2MP-TRX of affected flow r_i.

4) Constraints on Capacity of P2MP-TRXs:

$$z^{\mathrm{S}}_{v,p,i} = \tilde{z}^{\mathrm{S}}_{v,p,i}, \quad \{i: r_i\in\tilde{\mathbf{R}}\},\ \forall v\in V,\ p\in U^{\mathrm{H}}_v, \tag{21}$$

$$z^{\mathrm{E}}_{v,p,i} = \tilde{z}^{\mathrm{E}}_{v,p,i}, \quad \{i: r_i\in\tilde{\mathbf{R}}\},\ \forall v\in V,\ p\in U^{\mathrm{H}}_v, \tag{22}$$

$$\begin{aligned} &\begin{cases} \theta^{\mathrm{H}}_{v,p,i} \le z^{\mathrm{S}}_{v,p,i} \le \theta^{\mathrm{H}}_{v,p,i}\cdot M,\\ \theta^{\mathrm{H}}_{v,p,i} \le z^{\mathrm{E}}_{v,p,i} \le \theta^{\mathrm{H}}_{v,p,i}\cdot M,\\ z^{\mathrm{S}}_{v,p,i} \le C^{\mathrm{H}}_{v,p},\\ z^{\mathrm{E}}_{v,p,i} \le C^{\mathrm{H}}_{v,p},\\ 0 \le z^{\mathrm{E}}_{v,p,i} - z^{\mathrm{S}}_{v,p,i} \le \theta^{\mathrm{H}}_{v,p,i}\cdot M,\\ sc_i - M\cdot\left(1-\theta^{\mathrm{H}}_{v,p,i}\right) \le z^{\mathrm{E}}_{v,p,i} - z^{\mathrm{S}}_{v,p,i} + 1 \le sc_i, \end{cases}\\ &\{i: r_i\in\mathbf{R}\},\ \forall v\in V,\ p\in U^{\mathrm{H}}_v. \end{aligned} \tag{23}$$

Eq. (21)-Eq. (22) record the SCs used by each unaffected flow on its hub P2MP-TRX, and Eq. (23) ensures that the bandwidth of each affected flow can be supported by its hub P2MP-TRX.

$$\begin{aligned} &\begin{cases} 0 \le sc_{i,v,p} \le \theta^{\mathrm{L}}_{v,p,i}\cdot M,\\ C^{\mathrm{L}}_{v,p} - M\cdot\left(1-\theta^{\mathrm{L}}_{v,p,i}\right) \le sc_{i,v,p} \le C^{\mathrm{L}}_{v,p}, \end{cases}\\ &\{i: r_i\in\mathbf{R}\},\ \forall v\in V,\ p\in U^{\mathrm{L}}_v, \end{aligned} \tag{24}$$

$$\sum_{v\in V}\sum_{p\in U^{\mathrm{L}}_v} sc_{i,v,p} \ge sc_i, \quad \{i: r_i\in\mathbf{R}\}. \tag{25}$$

Eq. (24)-Eq. (25) ensure that the bandwidth of each affected flow can be supported by the leaf P2MP-TRXs assigned to it.

5) Constraints on SC Allocation:

$$\begin{aligned} &\begin{cases} \left(o^p_{i,j}-1\right)\cdot M + \alpha^p_{i,j} \le z^{\mathrm{S}}_{v,p,i} - z^{\mathrm{S}}_{v,p,j} \le o^p_{i,j}\cdot M - \alpha^p_{i,j},\\ \left(o^p_{i,j}-1\right)\cdot M + \alpha^p_{i,j} \le z^{\mathrm{S}}_{v,p,i} - z^{\mathrm{E}}_{v,p,j} \le o^p_{i,j}\cdot M - \alpha^p_{i,j},\\ \left(o^p_{i,j}-1\right)\cdot M + \alpha^p_{i,j} \le z^{\mathrm{E}}_{v,p,i} - z^{\mathrm{S}}_{v,p,j} \le o^p_{i,j}\cdot M - \alpha^p_{i,j}, \end{cases}\\ &\{i,j: r_i\in\mathbf{R}, r_j\in\mathbf{R}\cup\tilde{\mathbf{R}}, i\ne j, v=s_i\},\ \forall p\in U^{\mathrm{H}}_v. \end{aligned} \tag{26}$$

Eq. (26) determines the SCs used by each affected flow on its hub P2MP-TRX.

6) Constraints on Reconfiguring In-Service P2MP-TRXs:

$$\begin{cases} f^{\mathrm{H,S}}_{v,p} - \tilde{f}^{\mathrm{H,S}}_{v,p} \le \pi_{v,p}\cdot M,\\ \tilde{f}^{\mathrm{H,S}}_{v,p} - f^{\mathrm{H,S}}_{v,p} \le \pi_{v,p}\cdot M, \end{cases} \quad \forall v\in V,\ p\in\tilde{U}^{\mathrm{H}}_v, \tag{27}$$

$$\rho^{\mathrm{H}}_{v,p} \le f^{\mathrm{H,S}}_{v,p} \le \rho^{\mathrm{H}}_{v,p}\cdot M, \quad \forall v\in V,\ p\in U^{\mathrm{H}}_v\setminus\tilde{U}^{\mathrm{H}}_v. \tag{28}$$

Eq. (27) determines whether each previously-in-service hub P2MP-TRX on node v is reconfigured, and Eq. (28) identifies the start index of FS' used by each newly-activated hub P2MP-TRX on node v.

7) Constraints on Mapping SCs to FS':

$$\begin{aligned} &\begin{cases} 0 \le z^{\mathrm{S}}_{p,t,v,i} \le \xi^{\mathrm{H}}_{p,t,v}\cdot M,\\ z^{\mathrm{S}}_{v,p,i} - M\cdot\left(1-\xi^{\mathrm{H}}_{p,t,v}\right) \le z^{\mathrm{S}}_{p,t,v,i} \le z^{\mathrm{S}}_{v,p,i},\\ 0 \le z^{\mathrm{E}}_{p,t,v,i} \le \xi^{\mathrm{H}}_{p,t,v}\cdot M,\\ z^{\mathrm{E}}_{v,p,i} - M\cdot\left(1-\xi^{\mathrm{H}}_{p,t,v}\right) \le z^{\mathrm{E}}_{p,t,v,i} \le z^{\mathrm{E}}_{v,p,i},\\ \sum_{s\in N_p}\beta^{i,\mathrm{S}}_{t,p,v,s} \le 1,\ \sum_{s\in N_p}\beta^{i,\mathrm{S}}_{t,p,v,s}\cdot s = z^{\mathrm{S}}_{p,t,v,i},\\ \sum_{s\in N_p}\beta^{i,\mathrm{E}}_{t,p,v,s} \le 1,\ \sum_{s\in N_p}\beta^{i,\mathrm{E}}_{t,p,v,s}\cdot s = z^{\mathrm{E}}_{p,t,v,i}, \end{cases}\\ &\{i: r_i\in\mathbf{R}\},\ \forall v\in V,\ p\in U^{\mathrm{H}}_v,\ t\in T_{\mathrm{H}}, \end{aligned} \tag{29}$$

$$\begin{aligned} &\begin{cases} 0 \le f^{\mathrm{H,S}}_{v,p,i} \le M\cdot\theta^{\mathrm{H}}_{v,p,i},\\ f^{\mathrm{H,S}}_{v,p} - M\cdot\left(1-\theta^{\mathrm{H}}_{v,p,i}\right) \le f^{\mathrm{H,S}}_{v,p,i} \le f^{\mathrm{H,S}}_{v,p},\\ f^{\mathrm{S}}_{v,p,i} = f^{\mathrm{H,S}}_{v,p,i} + \sum_{t\in T_{\mathrm{H}}}\sum_{s\in N_p}\beta^{i,\mathrm{S}}_{t,p,v,s}\cdot\Delta f^{\mathrm{S}}_{t,s} - \theta^{\mathrm{H}}_{v,p,i},\\ f^{\mathrm{E}}_{v,p,i} = f^{\mathrm{H,S}}_{v,p,i} + \sum_{t\in T_{\mathrm{H}}}\sum_{s\in N_p}\beta^{i,\mathrm{E}}_{t,p,v,s}\cdot\Delta f^{\mathrm{E}}_{t,s} - \theta^{\mathrm{H}}_{v,p,i}, \end{cases}\\ &\{i: r_i\in\mathbf{R}\},\ \forall v\in V,\ p\in U^{\mathrm{H}}_v, \end{aligned} \tag{30}$$

$$\begin{cases} f^{\mathrm{S}}_{v,p,i} = f^{\mathrm{H,S}}_{v,p} + \tilde{f}^{\mathrm{S}}_i - 1,\\ f^{\mathrm{E}}_{v,p,i} = f^{\mathrm{H,S}}_{v,p} + \tilde{f}^{\mathrm{E}}_i - 1, \end{cases} \{i: r_i\in\tilde{\mathbf{R}}, v=s_i, p=\tilde{p}^{\mathrm{H}}_i\}. \tag{31}$$

Eq. (29)-Eq. (30) identify the FS' used by each affected flow on its restoration path, and Eq. (31) updates the FS' used by each unaffected flow if its lightpath is reconfigured after CLR.

8) Constraints on FS Allocation:

$$q^i_{u,v} = \tilde{q}^i_{u,v}, \quad \{i: r_i\in\tilde{\mathbf{R}}\},\ \forall u,v\in V, \tag{32}$$

$$\begin{aligned} &\begin{cases} 0 \le f^{\mathrm{S}}_{v,u,i} \le q^i_{v,u}\cdot M,\\ \sum_{v\in V}\sum_{p\in U^{\mathrm{H}}_v} f^{\mathrm{S}}_{v,p,i} - M\cdot\left(1-q^i_{v,u}\right) \le f^{\mathrm{S}}_{v,u,i} \le \sum_{v\in V}\sum_{p\in U^{\mathrm{H}}_v} f^{\mathrm{S}}_{v,p,i},\\ 0 \le f^{\mathrm{E}}_{v,u,i} \le q^i_{v,u}\cdot M,\\ \sum_{v\in V}\sum_{p\in U^{\mathrm{H}}_v} f^{\mathrm{E}}_{v,p,i} - M\cdot\left(1-q^i_{v,u}\right) \le f^{\mathrm{E}}_{v,u,i} \le \sum_{v\in V}\sum_{p\in U^{\mathrm{H}}_v} f^{\mathrm{E}}_{v,p,i}, \end{cases}\\ &\{i: r_i\in\mathbf{R}\cup\tilde{\mathbf{R}}\},\ \forall u,v\in V. \end{aligned} \tag{33}$$

Eq. (32) records the lightpath length of each unaffected flow, and Eq. (33) ensures the spectrum contiguous constraint for each lightpath after CLR.

$$p^{\mathrm{H}}_{v,u,i} = \tilde{q}^i_{v,u}\cdot\left[(|v|-1)\cdot|U^{\mathrm{H}}_v| + \tilde{p}^{\mathrm{H}}_i\right],\ \{i: r_i\in\tilde{\mathbf{R}}\},\ \forall u,v\in V, \tag{34}$$

$$\begin{cases} 0 \le p^{\mathrm{H}}_{v,u,i} \le q^{i}_{v,u} \cdot M, \\ \sum\limits_{v\in V}\sum\limits_{p\in U^{\mathrm{H}}_v} \theta^{\mathrm{H}}_{v,p,i} \cdot \left[(|v|-1)\cdot|U^{\mathrm{H}}_v|+p\right] - M\cdot\left(1-q^{i}_{v,u}\right), \\ \le p^{\mathrm{H}}_{v,u,i} \le \sum\limits_{v\in V}\sum\limits_{p\in U^{\mathrm{H}}_v} \theta^{\mathrm{H}}_{v,p,i} \cdot \left[(|v|-1)\cdot|U^{\mathrm{H}}_v|+p\right], \end{cases} \tag{35}$$

$$\{i : r_i \in \mathbf{R}\},\ \forall u, v \in V,$$

$$\begin{cases} 0 \le \gamma^{i,j}_{v,u}, \\ p^{\mathrm{H}}_{v,u,i} - p^{\mathrm{H}}_{v,u,j} \le \gamma^{i,j}_{v,u} \le p^{\mathrm{H}}_{v,u,i} - p^{\mathrm{H}}_{v,u,j} + M\cdot\delta^{i,j}_{v,u}, \\ p^{\mathrm{H}}_{v,u,j} - p^{\mathrm{H}}_{v,u,i} \le \gamma^{i,j}_{v,u} \le p^{\mathrm{H}}_{v,u,j} - p^{\mathrm{H}}_{v,u,i} + M\cdot\left(1-\delta^{i,j}_{v,u}\right), \\ \eta^{i,j}_{v,u} \le \gamma^{i,j}_{v,u} \le \eta^{i,j}_{v,u}\cdot M, \end{cases} \tag{36}$$

$$\{i, j : r_i \in \mathbf{R}\cup\tilde{\mathbf{R}}, r_j \in \mathbf{R}\cup\tilde{\mathbf{R}}, i \ne j\},\ \forall u, v \in V.$$

Eq. (34)-Eq. (35) determine the unique indices of the hub P2MP-TRXs used by unaffected and affected flows, where $|v|$ gets the unique index of node $v \in V$ and $|U^{\mathrm{H}}_v|$ returns the number of hub P2MP-TRXs in U^{H}_v, and Eq. (36) identifies whether flows using a same hub P2MP-TRX share fiber link $e = (v, u)$.

$$\begin{cases} \left(w^{i,j}_{v,u}-1\right)\cdot M + \eta^{i,j}_{v,u} \le f^{\mathrm{S}}_{v,u,i} - f^{\mathrm{S}}_{v,u,j} \le w^{i,j}_{v,u}\cdot M - \eta^{i,j}_{v,u}, \\ \left(w^{i,j}_{v,u}-1\right)\cdot M + \eta^{i,j}_{v,u} \le f^{\mathrm{S}}_{v,u,i} - f^{\mathrm{E}}_{v,u,j} \le w^{i,j}_{v,u}\cdot M - \eta^{i,j}_{v,u}, \\ \left(w^{i,j}_{v,u}-1\right)\cdot M + \eta^{i,j}_{v,u} \le f^{\mathrm{E}}_{v,u,i} - f^{\mathrm{S}}_{v,u,j} \le w^{i,j}_{v,u}\cdot M - \eta^{i,j}_{v,u}, \end{cases} \tag{37}$$

$$\{i, j : r_i \in \mathbf{R}\cup\tilde{\mathbf{R}}, r_j \in \mathbf{R}\cup\tilde{\mathbf{R}}, i \ne j\},\ \forall u, v \in V.$$

Eq. (37) ensures that the FS' used by flows sharing a same fiber link do not overlap.

9) Constraints on Statistical Results:

$$n^{\mathrm{H}}_t = \sum_{v\in V}\sum_{p\in U^{\mathrm{H}}_v} \xi^{\mathrm{H}}_{p,t,v} - \sum_{v\in V}\sum_{p\in \tilde{U}^{\mathrm{H}}_v} \tilde{\xi}^{\mathrm{H}}_{p,t,v}, \quad \forall t \in T_{\mathrm{H}}, \tag{38}$$

$$n^{\mathrm{L}}_t = \sum_{v\in V}\sum_{p\in U^{\mathrm{L}}_v} \xi^{\mathrm{L}}_{p,t,v} - \sum_{v\in V}\sum_{p\in \tilde{U}^{\mathrm{L}}_v} \tilde{\xi}^{\mathrm{L}}_{p,t,v}, \quad \forall t \in T_{\mathrm{L}}, \tag{39}$$

$$n_{\mathrm{FS}} = \sum_{v,u\in V}\sum_{\{i:r_i\in\mathbf{R}\cup\tilde{\mathbf{R}}\}} f^{\mathrm{E}}_{v,u,i} - f^{\mathrm{S}}_{v,u,i} + q^{i}_{v,u} - \mathcal{F}, \tag{40}$$

$$n_{\mathrm{R}} = \sum_{v\in V}\sum_{p\in U^{\mathrm{H}}_v} \pi_{v,p}, \tag{41}$$

Eq. (38)-Eq. (41) get the total numbers of newly-activated hub/leaf P2MP-TRXs of different types, new FS', and P2MP-TRX reconfigurations after CLR.

5. HEURISTIC ALGORITHM DESIGN

The ILP model formulated above rigorously describes how to recover a P2MP-TRX-based WSON from packet layer failure(s) with CLR, and the optimal solution can be obtained by solving it. However, solving the ILP will become intractable for large-scale problems. In this section, we propose a time-efficient heuristic to design cost-effective CLR quickly.

A. hHAG-DP for Cost-effective CLR

To restore all the affected traffic cost-effectively, our proposed heuristic (namely, hHAG-DP) combines hierarchical auxiliary graph (HAG) [11] and dynamic programming (DP), aiming to adopt the three CLR strategies adaptively. Specifically, we first traverse all the affected flows and build HAGs, trying to restore as many of them as possible with the first strategy, then leverage DP to maximize the utilization of in-service P2MP-TRXs' SCs by recovering affected flows with the second strategy, and finally activate idle P2MP-TRXs and set up new lightpaths to restore the remaining affected flows. *Algorithm 1* shows the overall procedure of hHAG-DP, where *Lines* 1-2 are for the initialization to prepare a temporary set $\mathbf{R}_h$ to store all the affected flows in $\mathbf{R}$.

A.1. HAG for First CLR Strategy

Lines 3-20 of *Algorithm 1* explain the sub-procedure of leveraging the first CLR strategy to restore affected flows. Specifically, for each affected flow r_i, we check the in-service hub P2MP-TRXs on its source s_i and build an HAG according to the current network status (*Line* 5), with which we try to restore r_i with the first CLR strategy in the best-effort way (*Lines* 6-18).

Algorithm 2 builds an HAG $G_{\mathrm{HAG}}(V_{\mathrm{HAG}}, E_{\mathrm{HAG}})$ for affected flow r_i. Here, *Line* 1 is for the initialization, and we denote the information about an in-service hub P2MP-TRX p on node s_i as $\{sc^{\mathrm{H}}_p, sc^{\mathrm{F}}_p\}$, where sc^{H}_p is the size of the largest available SC block on p and sc^{F}_p is the current central frequency of p. Then, the for-loop of *Lines* 2-11 checks each SC j on p to see whether the size of the largest available SC block starting from it can accommodate the bandwidth x_i of r_i. If yes, *Line* 5 first finds the FS block to carry the x_i SCs based on the current central frequency of p, and then *Lines* 6-8 iterate through all the fiber links in E and add a link in E_{HAG} if the FS block is available on it in $G(V, E)$. *Line* 12 returns the obtained HAG.

After obtaining the HAG $G_{\mathrm{HAG}}(V_{\mathrm{HAG}}, E_{\mathrm{HAG}})$, we use *Line* 6 in *Algorithm 1* to calculate the shortest path for $s_i \to d_i$ in it and record it as P. Note that, as the HAG already considers the FS usage in the P2MP-TRX-based WSON, r_i can be restored with P if P can be found in it, assuming that the required SCs do not increase on the restoration path P. Hence, *Line* 8 updates the required SCs according to the length of P. Then, if the number of required SCs of r_i does not increase, we just restore r_i with P using the first CLR strategy (*Lines* 9-12). Otherwise, we will update the number of required SCs and redo the procedure from Line 5 (*Lines* 13-16).

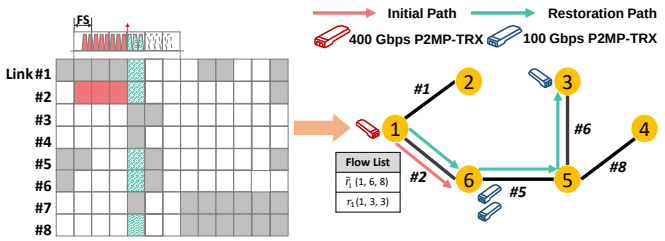

(a) Example on the first CLR strategy

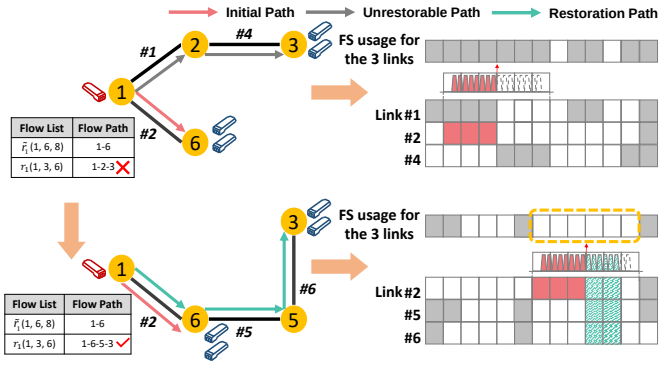

(b) Examples on the second and third CLR strategies

Fig. 4. Overall procedure of hHAG-DP.

Fig. 4(a) shows an example on using the first CLR strategy to restore an affected flow r_1 (1→3). There exists an in-service hub P2MP-TRX p at the source of r_1 (*Node* 1). Before the CLR, p has activated 8 SCs for the unaffected flow $\tilde{r}_1$ (1→6) and still

has 8 available SCs. Therefore, the first SC block that is available on p for restoring r_1 is *SCs* $[9, 11]$, since r_1 requires $x_1 = 3$ SCs. The left subplot of Fig. 4(a) shows the current FS usage in the P2MP-TRX-based WSON. It can be seen that based on the central frequency of p, its *SCs* $[9, 11]$ are mapped to use the 5-th FS, and *Links* 1, 2, 5, 6 and 8 have the 5-th FS available. Based on this, we build the HAG in the right subplot of Fig. 4(a), and the shortest path in it for 1→3 is 1→6→5→3. Finally, with the allocated SCs, FS′, and restoration path, we recover r_1 with the first CLR strategy.

Algorithm 1. Overall Procedure of hHAG-DP

1: $\mathbf{R}_h = \mathbf{R}$;
2: sort flows in $\mathbf{R}_h$ in ascending order of bandwidth;
3: **for** each flow $r_i \in \mathbf{R}_h$ **do**
4: **for** each in-service hub P2MP-TRX p at source s_i **do**
5: apply *Algorithm* 2 to build an HAG;
6: calculate the shortest path $s_i \rightarrow d_i$ in HAG as P;
7: **if** path P can be found **then**
8: get modulation format based on length of P, and update required SCs x_i' accordingly;
9: **if** $x_i' \leq x_i$ **then**
10: restore flow r_i with path P;
11: remove r_i from $\mathbf{R}_h$;
12: **break**;
13: **else**
14: **if** $x_i < x_i' \leq sc_p^{\mathrm{H}}$ **then**
15: $x_i = x_i'$, and go to *Line* 5;
16: **End**
17: **End**
18: **End**
19: **End**
20: **End**
21: divide $\mathbf{R}_h$ into sets $\{\mathbf{R}_h^{s_i}\}$ based on source s_i of each r_i;
22: **for** each nonempty set $\mathbf{R}_h^{s_i} \subseteq \mathbf{R}_h$ **do**
23: find each available SC block $a = \{\zeta_{p,s_i}^{\mathrm{S}}, sc_{p,s_i}\} \in A$ of each in-service hub P2MP-TRX p on node s_i;
24: sort the SC blocks in ascending order of sc_{p,s_i};
25: calculate K shortest paths for each affected flow in $\mathbf{R}_h^{s_i}$ in $G(V, E)$, get modulation format and required SCs on each path, and record path information in $\mathcal{P}$;
26: **for** each in-service hub P2MP-TRX p on node s_i **do**
27: **for** each available SC block $a \in A$ **do**
28: leverage knapsack-based DP to get the set of affected flows $\mathbf{R}_{a,p,s_i}$ can be restored with a;
29: $\mathbf{R}_h^{s_i} = \mathbf{R}_h^{s_i} \setminus \mathbf{R}_{a,p,s_i}$;
30: **End**
31: put unaffected flows using hub P2MP-TRX p in $\tilde{\mathbf{R}}_{p,s_i}$ and free FS′ used by them;
32: reconfigure hub P2MP-TRX p to reroute flows in $\mathbf{R}_{a,p,s_i} \cup \tilde{\mathbf{R}}_{p,s_i}$ based on path information in $\mathcal{P}$;
33: **End**
34: **while** $\mathbf{R}_h^{s_i} \neq \emptyset$ **do**
35: activate a hub P2MP-TRX p that can provide the SCs required by flows in $\mathbf{R}_h^{s_i}$;
36: leverage knapsack-based DP to get the set of affected flows $\mathbf{R}_{p,s_i}$ that can be restored with p;
37: $\mathbf{R}_h^{s_i} = \mathbf{R}_h^{s_i} \setminus \mathbf{R}_{p,s_i}$;
38: restore flows in $\mathbf{R}_{p,s_i}$ with p;
39: **End**
40: **End**
41: use *Algorithm* 3 to assign leaf P2MP-TRX(s) to each $r_i \in \mathbf{R}$;

A.2. Knapsack-based DP for Second and Third CLR Strategies

Lines 21-40 in *Algorithm* 1 describe the sub-procedures of applying the second and third CLR strategies. This time, each sub-procedure first determines the SC allocations and restoration paths of affected flows, and then finalizes their FS assignments as well as the center frequencies of used hub P2MP-TRXs. *Line* 21 divides the remaining affected flows into sets $\{\mathbf{R}_h^{s_i}\}$ based on the sources of affected flows. Then, the for-loop of *Lines* 22-40 processes each set $\mathbf{R}_h^{s_i}$ until all the affected flows have been restored.

Algorithm 2. Build HAG for an Affected Flow

Require: affected flow $r_i(s_i, d_i, x_i)$, in-service hub P2MP-TRX p on node s_i, and current network status of $G(V, E)$.
Ensure: HAG $G_{\mathrm{HAG}}(V_{\mathrm{HAG}}, E_{\mathrm{HAG}})$.
1: $V_{\mathrm{HAG}} = V$, $E_{\mathrm{HAG}} = \emptyset$;
2: **for** $j \in [1, sc_p^{\mathrm{H}} - x_i]$ **do**
3: find size ($sc_{s_i,p,j}$) of the largest available SC block on p starting from the j-th SC;
4: **if** $sc_{s_i,p,j} \geq x_i$ **then**
5: find FS block $[f_p^{\mathrm{S}}, f_p^{\mathrm{E}}]$ by mapping the available SC block of x_i SCs based on sc_p^{E};
6: **for** each fiber link $e \in E$ **do**
7: check FS usage on e in range $[f_p^{\mathrm{S}}, f_p^{\mathrm{E}}]$ and add e in $G_{\mathrm{HAG}}(V_{\mathrm{HAG}}, E_{\mathrm{HAG}})$ if the FS′ are available;
8: **End**
9: **break**;
10: **End**
11: **End**
12: **return** $G_{\mathrm{HAG}}(V_{\mathrm{HAG}}, E_{\mathrm{HAG}})$;

We first find all the available SC blocks on each in-service hub P2MP-TRX p on node s_i, record them in set A, and sort them in ascending order of their sizes to avoid SC fragmentation (*Lines* 23-24). Here, we denote each available SC block as $a = \{\zeta_{p,s_i}^{\mathrm{S}}, sc_{p,s_i}\}$, where $\zeta_{p,s_i}^{\mathrm{S}}$ and sc_{p,s_i} are the start index and size of the SC block. *Line* 25 calculates K shortest paths for each affected flow $r_i \in \mathbf{R}_h^{s_i}$ in the original topology $G(V, E)$, and records the information of the paths in set $\mathcal{P}$. Then, the for-loop of *Lines* 26-33 checks each in-service hub P2MP-TRX p on node s_i to restore as many affected flows in $\mathbf{R}_h^{s_i}$ as possible with the second CLR strategy. Specifically, we leverage knapsack-based DP to get the set of affected flows that can be restored with each SC block $a \in A$ (*Line* 28).

The knapsack-based DP works as follows. We treat the affected flows in $\mathbf{R}_h^{s_i}$ as items to be packed in the knapsack (*i.e.*, the available SC block a), each of which has a value of x_i (bandwidth demand of r_i in SCs), and thus the knapsack capacity is sc_{p,s_i}. Then, a two-dimensional (2D) DP array $\mathbf{K}[1, |\mathbf{R}_h^{s_i}|][1, sc_{p,s_i}]$ is introduced to solve the 0-1 knapsack problem. We first set all the elements in $\mathbf{K}$ to 0, then check whether $\mathbf{K}[i][1, j]$ can accommodate r_i and update $\mathbf{K}[i][1, sc_{p,s_i}]$ with the following recursive formula:

$$\mathbf{K}[i][j] = \begin{cases} \mathbf{K}[i-1][j], & x_i > j, \\ \max\left(\mathbf{K}[i-1][j], \mathbf{K}[i-1][j-x_i] + x_i\right), & x_i \leq j, \end{cases} \tag{42}$$

where x_i denotes the number of SCs required by r_i on the restoration path from hub P2MP-TRX p.

Fig. 4(b) gives an example on applying the second CLR strategy. This time, affected flow r_1 has $x_1 = 6$ SCs, and thus we need to allocate *FS′* $[5, 6]$ to restore it, according to the current central frequency of the in-service hub P2MP-TRX on *Node* 1. Then, based on the FS usage in the left subplot of Fig. 4(a), *FS′* $[5, 6]$ are only available on *Links* 1, 2, and 8, and thus we cannot find a restoration path for r_1 (1→3) with the HAG containing the three links. Therefore, we restore to DP and calculate the shortest path for r_1 in the original topology as 1→2→3. After combining

1→2→3 with the initial path of unaffected flow $\tilde{r}_1$ (1→6), we obtain three required links, *i.e.*, *Links* 1, 2 and 4. However, the FS usage on the three links does not provide enough available FS' for r_1 and $\tilde{r}_1$. Therefore, we proceed to check the second shortest path for r_1, *i.e.*, 1→6→5→3. Then, the required links become *Links* 2, 5 and 6, and the FS usage on them can provide enough available FS' for r_1 and $\tilde{r}_1$, *i.e.*, by reconfiguring the in-service hub P2MP-TRX on *Node* 1 to use *FS'* $[7, 12]$, we finish CLR.

If there are still affected flows that not been restored, the while-loop of *Lines* 34-39 in *Algorithm* 1 uses the third CLR strategy to recover them. Here, the procedure is similar to that of the second CLR strategy, except for that we use knapsack-based DP to get the set of affected flows that can be restored with each newly-activated hub P2MP-TRX (*Line* 36). As the procedures of the second and third strategies are similar, Fig. 4(b) can also explain how to apply the third strategy.

Algorithm 3. DP for Assigning Leaf P2MP-TRXs

1: $\mathbf{R}_l = \mathbf{R}$;
2: **for** each flow $r_i \in \mathbf{R}_l$ **do**
3: update bandwidth x_i of r_i based on its restoration path;
4: check all in-service leaf P2MP-TRXs on node d_i to get available SCs on them;
5: assign available SCs on in-service leaf P2MP-TRXs to receive as many contiguous SCs of r_i as possible;
6: record number of unserved SCs of r_i as x_i^*;
7: **if** $x_i^* > 0$ **then**
8: initialize a 2D DP array $\mathbf{K}[1, |T_L|][1, x_i^*] = \mathbf{0}$;
9: update $\mathbf{K}[1][1, x_i^*]$;
10: **for** $t \in [2, |T_L|]$ **do**
11: **for** $x \in [1, x_i^*]$ **do**
12: update $\mathbf{K}[t][x]$ with Eq. (43);
13: **End**
14: **End**
15: select idle leaf P2MP-TRXs on d_i to receive x_i^* SCs of r_i based on $\mathbf{K}[1, |T_L|][1, x_i^*]$;
16: **End**
17: **End**

A.3. Knapsack-based DP for Assigning Leaf P2MP-TRXs

Finally, *Line* 41 in *Algorithm* 1 assign leaf P2MP-TRX(s) on the destination d_i of each affected flow r_i to complete its CLR, by leveraging *Algorithm* 3. *Line* 1 is for the initialization, and then the for-loop of *Lines* 2-17 assign leaf P2MP-TRX(s) to each affected flow r_i. In each iteration, we first check whether the SCs of r_i can be received by the in-service leaf P2MP-TRXs on d_i (*Lines* 3-5). If not, we record the number of the remaining SCs of r_i as x_i^*, and select idle leaf P2MP-TRXs on d_i to receive them by leveraging the knapsack-based DP algorithm (*Lines* 6-16). We still introduce a 2D DP array $\mathbf{K}[1, |T_L|][1, x_i^*]$ to get the minimum costs and allocation schemes for leaf P2MP-TRXs, where $|T_L|$ is the number of the types of leaf P2MP-TRXs. *Line* 8 initializes $\mathbf{K}$ as $\mathbf{0}$, and *Line* 9 updates $\mathbf{K}[1][1, x_i^*]$ by calculating the cost of using type-1 leaf P2MP-TRXs to receive the remaining SCs. Next, we traverse $\mathbf{K}[t][x]$ to update its elements with the following recursive formula (*Lines* 10-14):

$$\mathbf{K}[t][x] = \begin{cases} \min(\mathbf{K}[t-1][x], \Delta_t), & x \le C_t, \\ \min(\mathbf{K}[t-1][x], \mathbf{K}[t][x - C_t] + \Delta_t), & x > C_t. \end{cases} \quad (43)$$

Finally, we select idle leaf P2MP-TRXs on d_i to receive x_i^* SCs of r_i based on the minimum costs in $\mathbf{K}[1, |T_L|][1, x_i^*]$.

B. Complexity Analytics

The overall time complexity of our hHAG-DP algorithm in *Algorithm* 1 is $O(|\mathbf{R}| \cdot \log_2(|\mathbf{R}|) + |\mathbf{R}| \cdot \hat{U}^H \cdot (\hat{C} + |E| \cdot F + (|V| + |E|) \log_2 |V|) + |V| \cdot (|A| \cdot \log_2(|A|) + K \cdot |V|(|V| + |E|) \log_2 |V| + \hat{U}^H + |A| \cdot |\mathbf{R}| \cdot \hat{C} + |\mathbf{R}|^2 \cdot \hat{C}) + |\mathbf{R}| \cdot |T_L| \cdot \hat{C})$, where $\hat{U}^H$ is the maximum number of hub P2MP-TRX per node and $\hat{C}$ is the largest SC capacity per hub/leaf P2MP-TRX.

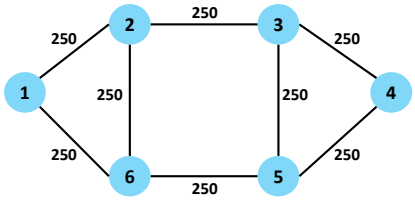

(a) 6-node topology

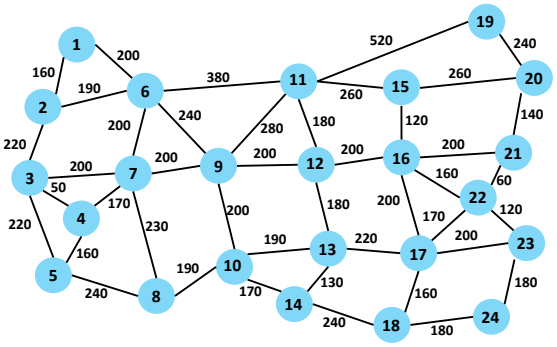

(b) USB topology

Fig. 5. Topologies used in simulations.

6. PERFORMANCE EVALUATION

In this section, we discuss the numerical simulations for evaluating our proposed algorithms.

A. Simulation Setup

The simulations consider the two topologies shown in Fig. 5, *i.e.*, a 6-node topology and the 24-node US Backbone (USB) topology. In the optical layer, each fiber link supports 358 FS', with each FS occupying 12.5 GHz of bandwidth [46]. We consider three types of P2MP-TRXs that accommodate 1/4/16 SCs (each SC occupies 4 GHz [13]) corresponding to 1/2/6 FS', and can achieve 25/100/400 Gbps rates in DP-16QAM [35], respectively. For traffic generation in each simulation [47], we randomly select the source and destination for each flow, set the bit-rate of each flow as $25 \cdot \lambda$ Gbps, and consider two traffic scenarios:

- Light traffic scenario: we set $\lambda \in [1, 4]$.
- Heavy traffic scenario: we set $\lambda \in [5, 8]$.

The total traffic volume was set properly to ensure that all the flows can be served or restored within the capacity limit, *i.e.*, no traffic blocking was introduced. We provisioned the traffic initially with an HAG-based approach. Specifically, we formed trees by checking the spectrum availability on each link and by calculating and merging the shortest paths over the residual graphs with affordable capacity. Transceiver allocation and RSA were then performed in a greedy or first-fit manner to minimize cost on transceiver and spectrum utilization (*i.e.*, without overprovisioning or spectrum fragmentation). In each simulation, we randomly selected a packet switch to fail to get the affected flows in $\mathbf{R}$ for CLR. For the unit costs of CLR, we

Table 1. Running Time of Algorithms in Light traffic scenario of Small-scale Simulations (seconds)

Total Demand	ILP			hHAG-DP	hHAG-C	HAG
in **R** (Gbps)	Variables	Constraints	Time	Time	Time	Time
100	62273	119075	11.3045	0.0718	0.1111	0.0446
200	108423	229680	94.4958	0.0906	0.7875	0.0567
300	184757	463673	681.3586	0.0679	0.0801	0.0619
400	205651	528146	904.4106	0.0778	0.0946	0.0771
500	276653	836872	32407.3383	0.0942	0.1103	0.1013

Table 2. Running Time of Algorithms in Heavy traffic scenario of Small-scale Simulations (seconds)

Total Demand	ILP			hHAG-DP	hHAG-C	HAG
in **R** (Gbps)	Variables	Constraints	Time	Time	Time	Time
200	39663	70656	1.2982	0.0284	0.0397	0.0292
400	88179	175363	8.4840	0.0455	0.0522	0.0445
600	138555	307408	532.7188	0.0580	0.0721	0.0616
800	173379	415163	852.1022	0.0823	0.0956	0.0902
1000	216470	566934	2122.6028	0.0918	0.1078	0.0940

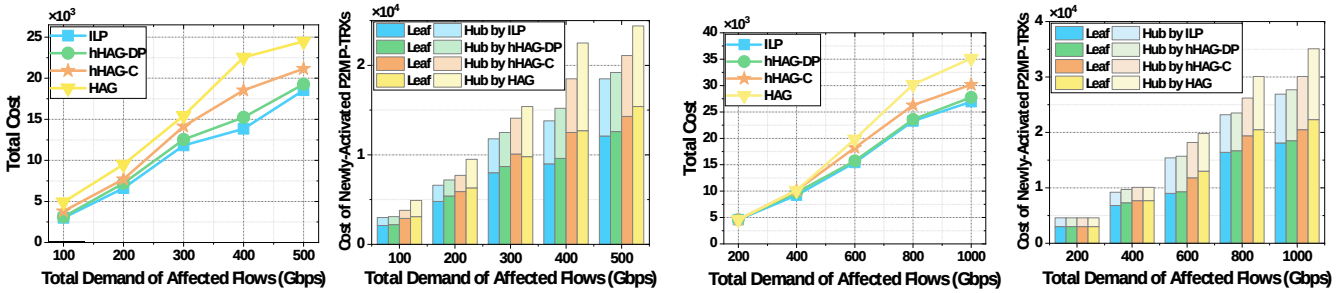

(a) Light traffic scenario (b) Heavy traffic scenario

Fig. 6. Costs in small-scale simulations.

set $\Delta_f = 1$, $\Delta_r = 100$, and the unit costs of 25/100/400 Gbps P2MP-TRXs as 1000/2000/4000, respectively, according to their complexity and availability [12, 29]. We set the K of K-shortest path routing used in the algorithms as $K = 3$.

The simulations compare four algorithms: 1) the ILP formulated in Section 4 (solved by Gurobi [48]), 2) the proposed hHAG-DP algorithm, 3) the hHAG-C algorithm in [29], and 4) a baseline HAG-based algorithm. hHAG-C restores affected traffic by combining HAG and aggregated Steiner tree, while HAG purely relies on HAGs to restore affected traffic. To ensure the statistical accuracy of results, we independently run 10 simulations and average the results for each data point. The simulations run on a server with 2.2 GHz Intel Xeon Silver 4210 CPU and 64 GB memory.

B. Small-Scale Simulations

We first conducted small-scale simulations on 6-node topology to compare the performance of ILP, hHAG-DP, hHAG-C, and HAG. We considered light and heavy traffic scenarios, where the total demand of affected flows (in terms of both absolute values in Gbps and percentage to the total traffic volume) is selected from {(100, 7.4%), (200, 10.5%), (300, 12.0%), (400, 12.7%), (500, 13.0%)} and {(200, 13.5%), (400, 20.2%), (600, 24.0%), (800, 25.2%), (1000, 26.0%)}, respectively. Fig. 6 shows the results on total CLR cost and cost of newly-activated P2MP-TRXs, where the results of light and heavy traffic scenarios are plotted in Figs. 6(a) and 6(b), respectively. Each datum in the figures was obtained by measuring the results from 10 independent runs to ensure sufficient statistical accuracy.

In the left subplot of Fig. 6(a), the ILP provides the lowest total cost, followed by hHAG-DP, hHAG-C, and finally HAG. Actually, when the total demand of affected traffic is 300 Gbps or less, the total cost from hHAG-DP is very close to the optimal solution from the ILP. As the total demand increases, the total costs from hHAG-C and HAG diverge more from the optimal solutions, but the performance gap between hHAG-DP and the

Table 3. Running Time of Algorithms in Large-scale Simulations (seconds)

Total Demand	*Light Traffic Scenario*			Total Demand	*Heavy Traffic Scenario*		
in **R** (Tbps)	hHAG-DP	hHAG-C	HAG	in **R** (Tbps)	hHAG-DP	hHAG-C	HAG
5	2.1806	2.0153	7.1899	5	1.3917	0.9872	2.8137
10	3.9637	2.2780	9.5747	10	2.7378	1.3973	6.6237
15	4.7461	3.1617	17.6315	15	3.3158	1.5165	11.9999
20	5.3646	4.0524	28.3434	20	3.8682	2.0475	17.9476
25	6.2464	5.5879	46.5694	25	4.6308	2.3208	25.8254

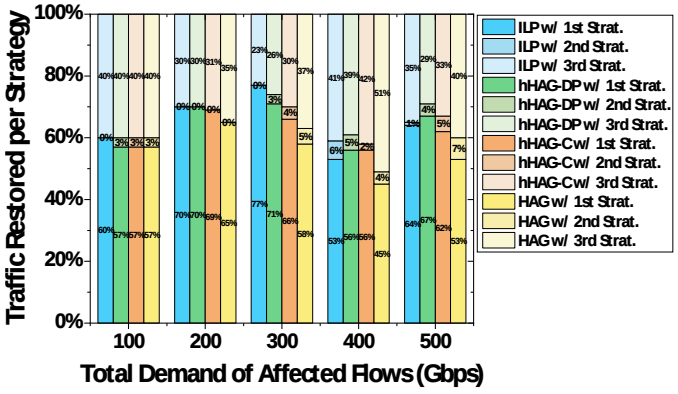

(a) Light traffic scenario

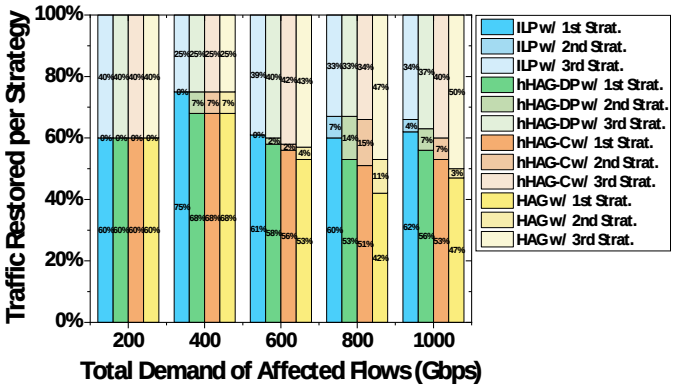

(b) Heavy traffic scenario

Fig. 7. Traffic restored per strategy in small-scale simulations.

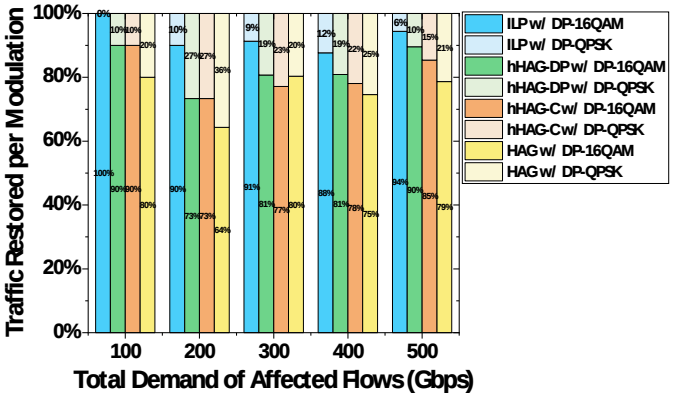

(a) Light traffic scenario

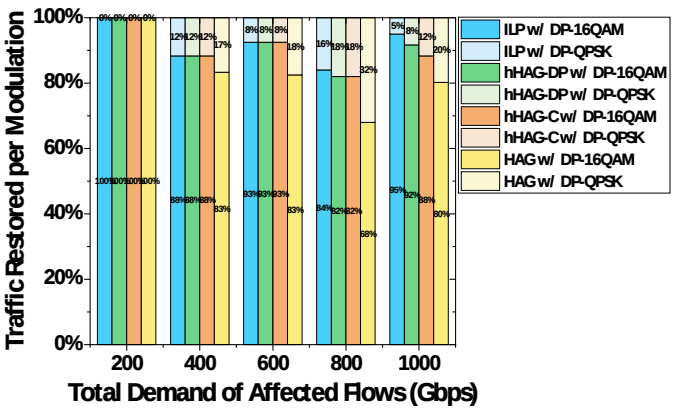

(b) Heavy traffic scenario

Fig. 8. Traffic restored per modulation in small-scale simulations.

ILP remains to be small, confirming the superiority of hHAG-DP. The rationale behind this can be found in the right subplot of Fig. 6(a). As newly-activated P2MP-TRXs contribute majorally to total CLR cost, reducing their number leads to effective cost-saving. Due to the fact that the DP algorithm in hHAG-DP can efficiently utilize the SCs in hub/leaf P2MP-TRXs, it activates fewer P2MP-TRXs than hHAG-C and HAG. The results in Fig. 6(b) show same trends as those in Fig. 6(a). Actually, in the heavy traffic scenario, the total cost from hHAG-DP becomes even closer to the optimal solution, further demonstrating its advantages.

Fig. 7 shows the proportion of affected flows restored by each strategy under different algorithms. We can see that the ILP generally relies on the first and second strategies to restore affected flows and save total CLR cost. However, for the light traffic scenario, the proportion of the third strategy used by the ILP can be higher than those from hHAG-DP and hHAG-C, when the total demand of affected flow is 400 or 500 Gbps. This is because the ILP tries to activate more low-cost P2MP-TRXs for cost-saving, resulting in an increase in the proportion of traffic recovered by the third strategy. Fig. 8 shows the percentages of traffic restored using different modulation formats. In both light and heavy traffic scenarios, the ILP restores the most affected flows using DP-16QAM, followed by hHAG-DP. The results indicate that the ILP and hHAG-DP can effectively optimize the rerouting paths to allow the use of higher-order modulation format for

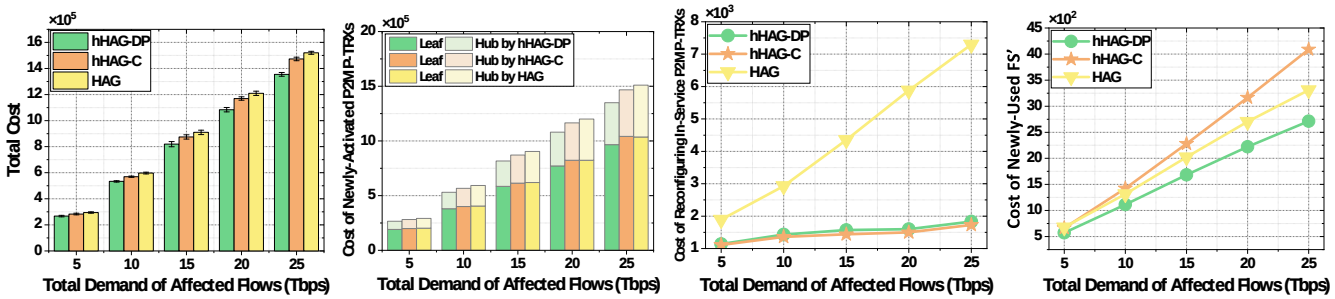

(a) Light traffic scenario

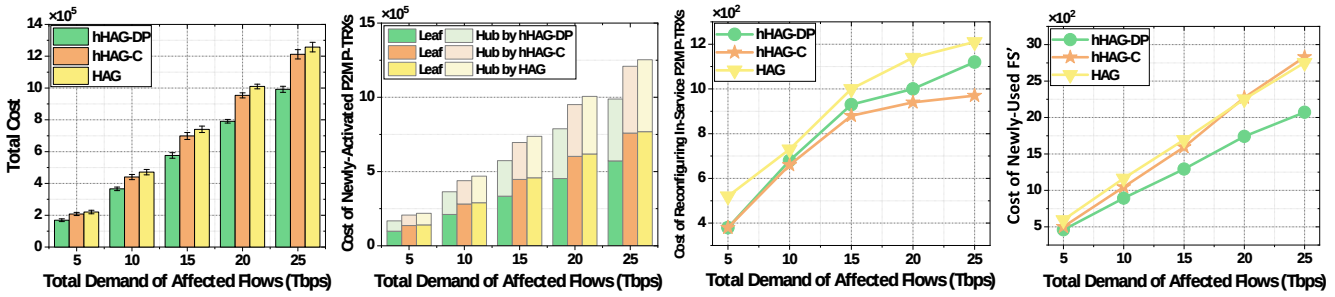

(b) Heavy traffic scenario

Fig. 9. Costs in large-scale simulations.

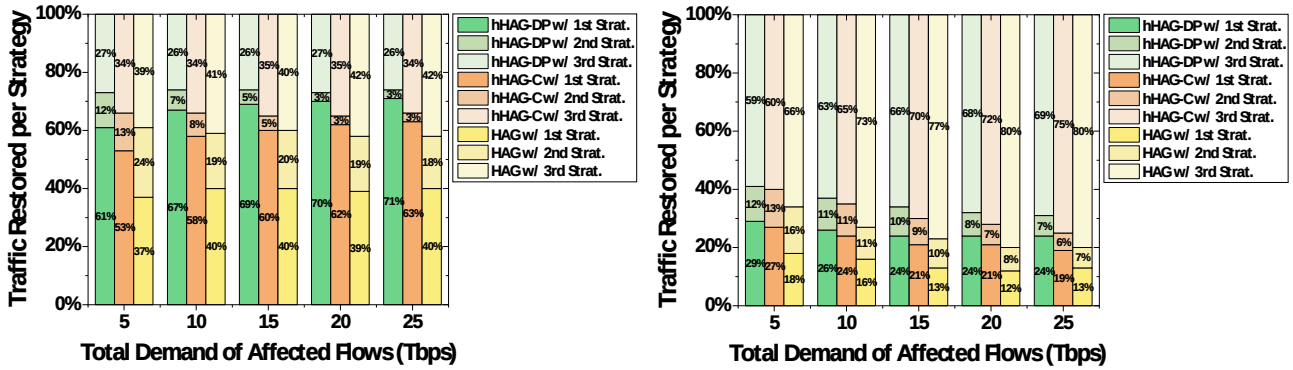

(a) Light traffic scenario (b) Heavy traffic scenario

Fig. 10. Traffic restored per strategy in large-scale simulations.

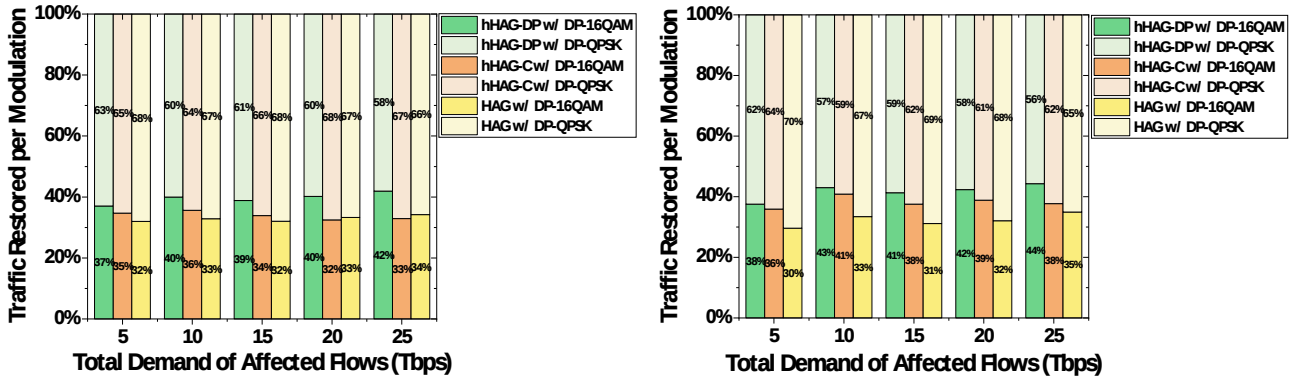

(a) Light traffic scenario (b) Heavy traffic scenario

Fig. 11. Traffic restored per modulation in large-scale simulations.

spectrum saving, and consequently, to decrease the likelihood of activating new P2MP-TRXs. Tables 1 and 2 summarize the running time of different algorithms in small-scale simulations. It can be observed that as the problem scale increases, the variables and constraints in the ILP grow, leading to an exponential increase in solution time, while in contrast, hHAG-DP can obtain near-optimal solutions within 0.1 second and its running time is shorter than that of hHAG-C and comparable to that of HAG.

C. Large-Scale Simulations

We conduct large-scale simulations on the USB topology. Due to the complexity of solving the ILP, we only consider the performance comparison of hHAG-DP, hHAG-C, and HAG. The total demand of affected flows is selected from {(5, 2.4%), (10, 2.8%), (15, 3.0%), (20, 3.2%), (25, 3.2%)} and {(5, 3.2%), (10, 4.4%), (15, 5.0%), (20, 5.4%), (25, 5.7%)} (in Tbps and percentage), for light and heavy traffic scenarios, respectively. Fig. 9 shows the results on total and itemized costs in the large-scale simulations, where the total costs are marked with 90% confidence intervals and three key cost components are highlighted in the subsequent subplots: the cost on newly-activated P2MP-TRXs, the cost on reconfiguring in-service P2MP-TRXs, and the cost on newly-used FS′.

In line with the trends in the small-scale simulations, Figs. 9(a) and 9(b) show hHAG-DP always achieves the lowest total costs, and its advantage over hHAG-C and HAG expands as the total demand in **R** increases. This is because hHAG-DP can effectively reduce the dominating cost on activating new P2MP-TRXs. HAG induces the highest cost on newly-activated P2MP-TRXs, and thereby, the highest total cost, while hHAG-C slightly transcends HAG. Next, by checking the cost on reconfiguring in-service P2MP-TRXs, we observe that hHAG-DP and hHAG-C largely beat HAG under the light traffic scenario. We attribute this phenomenon to the fact that hHAG-DP and hHAG-C prioritize allocating unused SCs by in-service P2MP-TRXs to the affected flows, allowing for restoring multiple flows concurrently. In contrast, HAG only recovers one affected flow at a time, unavoidably leading to excessive reconfigurations. The advantages of hHAG-DP and hHAG-C diminish under the heavy traffic scenario, because they can hardly restore multiple flows simultaneously in this case. Although the cost of newly-used FS′ has the smallest impact on the total cost, we still find that hHAG-DP always incurs lower FS cost than hHAG-C and HAG.

The proportion of affected flows recovered by each strategy is shown in Fig. 10. By fully utilizing the in-service P2MP-TRXs, hHAG-DP enables the most affected flows to be recovered by the more cost-effective first and second strategies, echoing the results in Fig. 9. The superiority of hHAG-DP can be further revealed by the results on the percentage of traffic restored using different modulation formats in Fig. 11. We can see that hHAG-DP restores the most affected flows using DP-16QAM and presents a definite advantage in spectrum efficiency. Table 3 lists the running time of the algorithms in large-scale simulations. Both hHAG-DP and hHAG-C can complete the calculation within 10 seconds due to their ability to simultaneously restore multiple flows, whereas HAG needs more than 46 seconds in the worst case.

7. CONCLUSION

We studied how to recover a P2MP-TRX-based WSON from packet layer failure(s) cost-effectively with well-designed CLR. Based on the characteristics of P2MP-TRXs, we first designed three CLR strategies to achieve cost-effective restoration of affected flows by fully utilizing SCs on P2MP-TRXs and FS′ on fiber links. Then, we formulated a rigorous ILP model to define the problem with the objective of minimizing the cost introduced during CLR. Next, we proposed a time-efficient heuristic, namely, hHAG-DP, to find near-optimal CLR schemes quickly. Extensive simulations indicated that our proposal provides results close to the optimal solutions from the ILP and outperform existing benchmarks. Future research directions include: 1) investigations of applying multipath routing, free SC capacities and transceiver type/role switching in traffic restoration, and 2) studies considering more advanced P2MP-TRX configurations (*e.g.*, 100/400/800 Gbps).

FUNDING

This work was supported by the NSFC project 62371432.

REFERENCES

1. P. Lu, L. Zhang, X. Liu, J. Yao, and Z. Zhu, "Highly-efficient data migration and backup for Big Data applications in elastic optical inter-datacenter networks," IEEE Netw. **29**, 36–42 (2015).
2. W. Lu, Z. Zhu, and B. Mukherjee, "On hybrid IR and AR service provisioning in elastic optical networks," J. Light. Technol. **33**, 4659–4669 (2015).
3. K. Wu, P. Lu, and Z. Zhu, "Distributed online scheduling and routing of multicast-oriented tasks for profit-driven cloud computing," IEEE Commun. Lett. **20**, 684–687 (2016).
4. J. Liu, W. Lu, F. Zhou, P. Lu, and Z. Zhu, "On dynamic service function chain deployment and readjustment," IEEE Trans. Netw. Serv. Manag. **14**, 543–553 (2017).
5. W. Lu, L. Liang, B. Kong, B. Li, and Z. Zhu, "AI-assisted knowledge-defined network orchestration for energy-efficient data center networks," IEEE Commun. Mag. **58**, 86–92 (2020).
6. "Cisco annual internet report, (2018-2023)," https://www.cisco.com/c/en/us/solutions/collateral/executive-perspectives/annual-internet-report/white-paper-c11-741490.html.
7. J. Navarro-Ortiz, P. Romero-Diaz, S. Sendra, P. Ameigeiras, J. Ramos-Munoz, and J. Lopez-Soler, "A survey on 5G usage scenarios and traffic models," IEEE Commun. Surv. Tuts. **22**, 905–929 (2020).
8. Z. Zhu, W. Lu, L. Zhang, and N. Ansari, "Dynamic service provisioning in elastic optical networks with hybrid single-/multi-path routing," J. Light. Technol. **31**, 15–22 (2013).
9. L. Gong, X. Zhou, X. Liu, W. Zhao, W. Lu, and Z. Zhu, "Efficient resource allocation for all-optical multicasting over spectrum-sliced elastic optical networks," J. Opt. Commun. Netw. **5**, 836–847 (2013).
10. Y. Yin, H. Zhang, M. Zhang, M. Xia, Z. Zhu, S. Dahlfort, and S. Yoo, "Spectral and spatial 2D fragmentation-aware routing and spectrum assignment algorithms in elastic optical networks," J. Opt. Commun. Netw. **5**, A100–A106 (2013).
11. L. Gong and Z. Zhu, "Virtual optical network embedding (VONE) over elastic optical networks," J. Light. Technol. **32**, 450–460 (2014).
12. D. Welch *et al.*, "Point-to-multipoint optical networks using coherent digital subcarriers," J. Light. Technol. **39**, 5232–5247 (2021).
13. D. Welch *et al.*, "Digital subcarrier multiplexing: Enabling software-configurable optical networks," J. Light. Technol. **41**, 1175–1191 (2023).
14. M. Hosseini, J. Pedro, A. Napoli, N. Costa, J. Prilepsky, and S. Turitsyn, "Multi-period planning in metro-aggregation networks exploiting point-to-multipoint coherent transceivers," J. Opt. Commun. Netw. **15**, 155–162 (2023).
15. C. Tremblay, E. Archambault, R. Wilson, S. Clelland, M. Furdek, and L. Wosinska, "Agile metropolitan filterless optical networking," in *Proc. of FNWF 2022*, (2022), pp. 113–116.
16. Q. Lv, R. Li, and Z. Zhu, "On the survivable multilayer planning of filterless optical networks with P2MP transceivers," J. Light. Technol. **42**, 1786–1797 (2024).

17. M. P. Fok, Z. Wang, Y. Deng, and P. R. Prucnal, "Optical layer security in fiber-optic networks," IEEE Trans. Inf. Forensics Secur. **6**, 725–736 (2011).
18. Q. Lv and Z. Zhu, "On the multilayer planning of filterless optical networks with OTN encryption," IEEE/ACM Trans. Netw. **31**, 2529–2544 (2023).
19. Y. Zhang, Q. Lv, R. Li, X. Tian, and Z. Zhu, "Planning of survivable wavelength-switched optical networks based on P2MP transceivers," IEEE Trans. Netw. Serv. Manag. **20**, 2331–2342 (2023).
20. P. Pavon-Marino, N. Skorin-Kapov, and A. Napoli, "Tree-determination, routing, and spectrum assignment using point-to-multipoint coherent optics," J. Opt. Commun. Netw. **15**, C29–C40 (2023).
21. R. Li, Q. Lv, and Z. Zhu, "On the network planning of wavelength switched optical networks with P2MP transceivers," J. Light. Technol. **42**, 24–36 (2024).
22. Z. Zhu, V. Hernandez, M. Jeon, J. Cao, Z. Pan, and S. Yoo, "RF photonics signal processing in subcarrier multiplexed optical-label switching communication systems," J. Light. Technol. **21**, 3155–3166 (2003).
23. Z. Pan, H. Yang, J. Yang, J. Hu, Z. Zhu, J. Cao, K. Okamoto, S. Yamano, V. Akella, and S. Yoo, "Advanced optical-label routing system supporting multicast, optical TTL, and multimedia applications," J. Light. Technol. **23**, 3270–3281 (2005).
24. Y. Zhang, M. O'Sullivan, and R. Hui, "Digital subcarrier multiplexing for flexible spectral allocation in optical transport network," Opt. Express **19**, 21880–21889 (2011).
25. "Finisar dual and quad wavelength selective switch (WSS)," https://finisarwss.com/wp-content/uploads/2020/07/FinisarWSS_Dual_Wavelength_Selective_Switch_ProductBrief_Jul2020.pdf.
26. Z. Zhu, M. Funabashi, Z. Pan, B. Xiang, L. Paraschis, and S. Yoo, "Jitter and amplitude noise accumulations in cascaded all-optical regenerators," J. Light. Technol. **26**, 1640–1652 (2008).
27. Z. Zhu, X. Chen, F. Ji, L. Zhang, F. Farahmand, and J. Jue, "Energy-efficient translucent optical transport networks with mixed regenerator placement," J. Light. Technol. **30**, 3147–3156 (2012).
28. B. Niu, J. Kong, S. Tang, Y. Li, and Z. Zhu, "Visualize your IP-over-optical network in realtime: A P4-based flexible multilayer in-band network telemetry (ML-INT) system," IEEE Access **7**, 82413–82423 (2019).
29. M. Wu, Y. Zhang, R. Li, Q. Lv, S. Li, and Z. Zhu, "Cross-layer restoration to resolve packet layer outages in P2MP-TRX-based WSONs," in *Proc. of OECC 2024,* (2024), pp. 1–3.
30. R. Govindan, I. Minei, M. Kallahalla, B. Koley, and A. Vahdat, "Evolve or die: High-availability design principles drawn from Google's network infrastructure," in *Proc. of ACM SIGCOMM 2016,* (2016), pp. 58–72.
31. A. Raj and O. Ibe, "A survey of IP and multiprotocol label switching fast reroute schemes," Comput. Netw. **51**, 1882–1907 (2007).
32. S. Liu, W. Lu, and Z. Zhu, "On the cross-layer orchestration to address IP router outages with cost-efficient multilayer restoration in IP-Over-EONs," J. Opt. Commun. Netw. **10**, A122–A132 (2018).
33. M. Wu, N. da Fonseca, and Z. Zhu, "Dynamic cross-layer restoration to resolve packet layer outages in FlexE-Over-EONs," IEEE Trans. Netw. Serv. Manag. **19**, 2600–2611 (2022).
34. M. Hosseini, J. Pedro, A. Napoli, N. Costa, J. Prilepsky, and S. Turitsyn, "Optimized design of filterless horseshoe networks exploiting point-to-multipoint coherent transceivers," J. Opt. Commun. Netw. **15**, 569–578 (2023).
35. P. Pavon-Marino *et al.*, "On the benefits of point-to-multipoint coherent optics for multilayer capacity planning in ring networks with varying traffic profiles," J. Opt. Commun. Netw. **14**, B30–B44 (2022).
36. C. Castro *et al.*, "Scalable filterless coherent point-to-multipoint metro network architecture," J. Opt. Commun. Netw. **15**, B53–B66 (2023).
37. M. Hosseini, J. Pedro, A. Napoli, N. Costa, J. Prilepsky, and S. Turitsyn, "Optimization of survivable filterless optical networks exploiting digital subcarrier multiplexing," J. Opt. Commun. Netw. **14**, 586–594 (2022).
38. L. Velasco *et al.*, "Autonomous and energy efficient lightpath operation based on digital subcarrier multiplexing," IEEE J. Sel. Areas Commun. **39**, 2864–2877 (2021).
39. Y. Fan *et al.*, "Point-to-multipoint coherent architecture with joint resource allocation for B5G/6G fronthaul," IEEE Wirel. Commun. **29**, 100–106 (2022).
40. J. Hernandez, F. Arpanaei, A. Napoli, C. Castro, O. de Dios, and J. Fernandez-Palacios, "On clustering coherent optics point-to-multipoint trees for cost-effective bandwidth assignment in MANs," J. Opt. Commun. Netw. **15**, 155–162 (2023).
41. R. Li, S. Li, M. Wu, Y. Zhang, L. Q., and Z. Zhu, "Dynamic asymmetric SC allocation and reconfiguration in drop-and-continue optical networks based on P2MP-TRXs," in *Proc. of OFC 2024,* (2024), pp. 1–3.
42. F. Ji, X. Chen, W. Lu, J. Rodrigues, and Z. Zhu, "Dynamic p-cycle protection in spectrum-sliced elastic optical networks," J. Light. Technol. **32**, 1190–1199 (2014).
43. X. Chen, F. Ji, and Z. Zhu, "Service availability oriented p-cycle protection design in elastic optical networks," J. Opt. Commun. Netw. **6**, 901–910 (2014).
44. X. Chen, M. Tornatore, F. Ji, W. Zhou, C. Chen, D. Hu, S. Zhu, L. Jiang, and Z. Zhu, "Flexible availability-aware differentiated protection in software-defined elastic optical networks," J. Light. Technol. **33**, 3872–3882 (2015).
45. X. Chen, S. Zhu, L. Jiang, and Z. Zhu, "On spectrum efficient failure-independent path protection p-cycle design in elastic optical networks," J. Light. Technol. **33**, 3719–3729 (2015).
46. L. Gong, X. Zhou, W. Lu, and Z. Zhu, "A two-population based evolutionary approach for optimizing routing, modulation and spectrum assignments (RMSA) in O-OFDM networks," IEEE Commun. Lett. **16**, 1520–1523 (2012).
47. H. Liang, N. da Fonseca, and Z. Zhu, "On the cross-layer network planning for flexible ethernet over elastic optical networks," IEEE Trans. Netw. Serv. Manag. **18**, 3691–3705 (2021).
48. "gurobi," https://www.gurobi.com/.